Journal of Catalysis 271 (2010) 290–304

Contents lists available at ScienceDirect

Journal of Catalysis

journal homepage: www.elsevier.com/locate/jcat

New rare earth oxide catalysts for the transesterification of triglycerides with methanol resulting in biodiesel and pure glycerol

Bernhard M.E. Russbueldt [a], Wolfgang F. Hoelderich [a,*]

[a] Department of Chemical Technology and Heterogeneous Catalysis, University of Technology RWTH Aachen, Worringerweg 1, D-52074 Aachen, Germany

ARTICLE INFO

Article history:
Received 16 December 2009
Revised 1 February 2010
Accepted 2 February 2010
Available online 20 March 2010

Keywords:
Biodiesel
Glycerol
Transesterification
Heterogeneous base catalysis
Rare earth oxides

ABSTRACT

The transesterification of different oils and fats with methanol in the presence of various rare earth oxide (REO) containing heterogeneous catalysts was investigated. Pure rare earth oxides, supported rare earth oxides, and stoichiometric rare earth mixed oxide catalysts were prepared. The catalysts were characterized by X-ray powder diffraction (XRD), nitrogen adsorption isotherm (BET), thermogravimetric analysis (TGA), and temperature-programmed desorption of CO_2 (TPD). The correlation of the catalyst structure and activity in batch wise lab-scale autoclave experiments was studied. Among the pure rare earth oxides, an exceptionally high activity was found for lanthanum oxide. Rare earth oxides on oxidic carriers lead to the formation of surface mixed oxide phases, while activated carbon enables to enhance the dispersion of the lanthanum oxide phase. A series of rare earth aluminates, titanates, and zirconates were prepared by flash combustion synthesis and a comparison of the surface activity is given.

1. Introduction

The growing energy demand of mankind has diminished the fossil energy sources and caused an alarming increase in CO_2 in the atmosphere. Therefore, the conversion of biomass into renewable transportation fuels is receiving more and more attention [1,2]. At present, the production of biomethane from cellulose [3], the fermentation of glucose and starch to bioethanol [4], and the conversion of fats and oils into biodiesel [5,6] are state of the art.

In future, the pyrolysis of triglycerides [7] or the decarboxylation of free fatty acids [8] into biodiesel might become practicable. The conversion of lignocellulose via syngas formation and Fischer–Tropsch synthesis as biomass to liquid fuels (BTL) is a current topic of research [9]. Finally, as an alternative to the conventional petrorefinery the term biorefinery was created [10–12], comprising the integrated production of energy, fuels, and platform chemicals with maximum overall efficiency and CO_2 net savings.

Currently, biodiesel is made by transesterification of natural triglycerides with methanol and a homogeneous base catalyst like NaOH or $NaOCH_3$, yielding a mixture of long-chained fatty acid methyl esters (FAME) [13,14]. The optimization of the reaction conditions was reviewed [15–19]. In addition, 10–12% glycerol related to the FAME output as by-product is obtained.

Disadvantageous is the high triglyceride quality, which is always in competition with food uses [20]. Fats and oils with a low content of free fatty acids (FFA) are required to avoid soap formation and serious problems due to emulsion formation [21]. During the biodiesel work-up, the base catalyst is neutralized by mineral acids and the salts formed end up in the glycerol. The crude glycerol is of low quality and value or requires costly purification by distillation. Glycerol is an important commodity chemical with several direct uses. Due to the fast-growing biodiesel industry, glycerol is becoming an important building block [22,23] for the production of acrylic acid [24] and acrolein [25,26]. Furthermore, glycerol can be converted into epichlorohydrin by the Epicerol process of Solvay or by proprietary Dow technology [23]. Moreover, 1,3-propandiol is accessible via combined hydration and hydrogenation of acrolein as shown by Evonik Degussa AG or directly from glycerol via an enzymatic route developed by Dow [22].

There is a need for a more benign and integrated biodiesel process, using low-quality fats and oils with high FFA level and producing cost-efficient biodiesel and high-quality glycerol. The use of heterogeneous catalysis [27–30] is a key technology to overcome such problems. The low end of pipe costs, energy savings, high efficiency, and selectivity are especially strong driving forces behind the development of new green and sustainable technologies [31–33].

Low-quality triglycerides can be used for the base-catalyzed transesterification only after removal of the FFA by refining. However, a preesterification of the FFA with methanol is preferred, because additional FAME is formed. The preesterification is accelerated by homogeneous acid catalysts [34–36] or more

* Corresponding author. Fax: +49 241 8022291.
E-mail addresses: hoelderich@rwth-aachen.de, whoelderich@rwth-aachen.de (W.F. Hoelderich).

0021-9517/$ - see front matter © 2010 Elsevier Inc. All rights reserved.
doi:10.1016/j.jcat.2010.02.005

advantageously by heterogeneous acid catalysts like ion exchange resins [37–40].

The only heterogeneously catalyzed transesterification process in practice was developed by the Institut Francais du Petrole (IFP) [41,42] and is commercialized by Axens as the EsterFip-H process. A basic spinel catalyst containing $Al_2O_3/ZnAl_2O_4/ZnO$ is used. A low FFA containing feedstock is required to avoid zinc soap formation. Diester Industries is running successfully two 160,000 t/a plants in France and Sweden, and further units are under construction [43]. Glycerol of >98% purity is produced, a great improvement compared to the 85% purity typical for the conventional process.

In recent years, the interest in the heterogeneously catalyzed transesterification increased and numerous catalysts, both acid and base, have been suggested [18,19,44–46]. However, the high molar mass of triglycerides and the operation in the liquid phase cause serious problems. The use of heterogeneous catalysts was shown to be mass transfer limited, causing a poor catalyst efficiency [47,48].

As base catalysts, the alkali metal oxides Li_2O, Na_2O, or K_2O on γ-Al_2O_3 were prepared by impregnation of high surface supports with the corresponding hydroxides [49], carbonates [50], nitrates [51,52], fluorides [53], or iodides [54] followed by activation typically at 500 °C. The spinel phase $LiAl_5O_8$ or orthoaluminates such as $NaAlO_2$ are formed on the surface. However, for most supported alkali metal catalysts leaching of alkali metal hydroxides causes problems. Partial homogeneous catalysis and catalyst deactivation was reported [49,55,56]. The same problems were observed for LiF, KF, and CsF on γ-Al_2O_3 [57].

A number of publications deal with alkaline earth metal oxides as catalysts. Among these, SrO and BaO are too highly soluble in methanol [58]. Despite that fact, CaO was recommended as a heterogeneous catalyst by a number of researchers [59,60] and later leaching and partial homogeneous catalysis was noted [61–63]. For MgO a high influence of the crystal morphology on the activity was reported [64,65]. Recently, the use of alkaline earth metal oxides, hydroxides, and carbonates and especially MgO and $CaCO_3$ as heterogeneous catalysts was patented [66]. Hydrotalcite $Mg_6Al_2(OH)_{16}CO_3{\cdot}4H_2O$ [67–69], MgO, and CaO on γ-Al_2O_3 [56,70] and perovskites like $CaTiO_3$, $CaMnO_3$, and $CaZrO_3$ [71] were also investigated.

The doping of MgO and CaO with Li_2O, Na_2O, or K_2O increases the base strength by replacement of alkaline earth metal cations by alkali metal cations and creation of oxygen vacancies [50]. Best results were reported for Li_2O-doped MgO and CaO [51], but the Li is not tightly enough bound to the host lattice [72]. In the same manner, KF/MgO was investigated [73].

Recently, rare earth oxide containing catalyst like Eu_2O_3/γ-Al_2O_3 [74], KF/Eu_2O_3 [75], La_2O_3/MgO [76], La_2O_3/CaO [77], and La_2O_3/ZnO [78] have been reported as transesterification catalysts. However, La_2O_3 was only used as a dopant to enhance the well-known activity of MgO, CaO, and ZnO. Furthermore, Eu_2O_3 is too expensive by far for an industrial application.

The activity of ZnO has already been mentioned, and CaO/ZnO mixed oxides have also been studied recently [79]. In the same manner, pure SnO [80] or SnO supported on γ-Al_2O_3 [81] are of high activity. Alkali metal oxide occluded zeolites like Na_2O/NaX faujasite [82] and $K_2O/SBA15$ [83] have been suggested, and titania silicalites like ETS-4 and ETS-10 and the titania zeolite ETAS-10 have been patented [84]. Polystyrene-bounded alkylguanidines serve as another alternative [85]. Anion exchange resins [86–88] and zinc and cadmium arginate [89,90] have been patented.

The best option would be a hybrid process by means of an acid catalyzed simultaneous FFA preesterification and triglyceride transesterification. For example, homogeneous acids like H_2SO_4 [91] and p-TsOH [34] or preferably heterogeneous acid catalysts should be used.

Cation exchange resins exhibit too low activity [92]. Sulfated zirconia SO_4^{2-}/ZrO_2 [93,94] leaches H_2SO_4, causing partial homogeneous activity. Heteropolyacids like $H_3PW_{12}O_{40}$ and $H_4SiW_{12}O_{40}$ are active, but could not be adequately immobilized on a support [95,96]. The corresponding salts like $Cs_{2.5}H_{1.5}SiW_{12}O_{40}$ [97] and $Zn_{1.2}H_{0.6}PW_{12}O_{40}$ [98] were also investigated. Montmorillonite clays are of low activity [99,100]. Finally, TiO_2-, Al_2O_3-, and WO_3-doped ZrO_2 indicated good activity and stability for both esterification and transesterification in long-term experiments [101].

However, for the hybrid process, the esterification proceeds much faster than the transesterification and the problem can be reduced to an acid transesterification. Due to the high reaction temperatures required, by-products like dimethylether, glycerol methylethers, and acrolein are formed. Since acid catalysis is much less efficient for the transesterification in comparison with basic catalysis, a two-step acid preesterification and basic transesterification process is favored for the processing of low-quality oils and fats.

Additionally, the enzymatic preesterification and transesterification was considered and patented [102,103]. A great number of enzymes were screened [104]. The low space time yield, the conformational enzyme destruction by excess methanol, and enzyme poisoning by phospholipides cause serious problems [105,106]. Nevertheless, in 2008 a 20,000 t/a pilot plant using immobilized enzymes started up in China [104].

Process engineering developments include the addition of co-solvents like MTBE [107] or propane [108]. The transition from a heterogeneous two liquid phase mixture to a homogeneous system eliminates phase transition limitations and accelerates the rate of the reaction. The same effect can be achieved by working in supercritical methanol [109,110]. The non-catalytic reaction becomes fast enough, but the high temperature, pressure, and by-product formation are disadvantageous.

The aim of this work was to study rare earth oxides, their supported oxides, and rare earth metal mixed oxides as catalysts for the transesterification of triglycerides with methanol into biodiesel. The lanthanide element series offers the unique opportunity to infinitely tune and optimize the basicity of heterogeneous catalysts. Structure–activity relationships can be thoroughly investigated.

2. Experimental

2.1. Materials

Rapeseed oil was kindly provided from Biowerk Sohland GmbH, Germany, and both crude and refined palm oil from ADM Company, Germany.

Generous amounts of $Zr(OH)_4$ XZO1247/01, $Zr(OH)_4$/10% La_2O_3 XZO 1526/01, and $Zr(OH)_4$/8% Y_2O_3 XZO 1523/01 were obtained from Mel Chemicals, England, and we are very grateful for that.

As catalyst support γ-Al_2O_3 Type C of Evonik Degussa AG, Germany was used.

Ammonia 25% (p.a.), $Al(NO_3)_3{\cdot}9H_2O$ (99%), methanol (99.8%), nitric acid 65% (p.a.), oxalic acid dihydrate (99%), pyridine (99.5%), and urea (99.5%) were purchased from Merck; N,O-bis-(trimethylsilyl)-trifluoracetamide (BSTFA) (97%) and all rare earth oxides (99.9%) from ABCR; methylheptadecanoate (99.7%), tricaprin (99.0%), and activated carbon (analytical grade made from wood) from Fluka; $TiCl_4$ (99%) from Acros; and $La(NO_3)_3{\cdot}6H_2O$ (99%) and $Ce(NO_3)_3{\cdot}6H_2O$ (99%) from Aldrich.

2.2. Catalyst preparation

2.2.1. Pure rare earth oxides

For example, 16.29 g La_2O_3 (0.05 mol) is dissolved in 22.9 ml 65% HNO_3 (0.33 mol) and diluted with distilled water to 500 ml.

A solution of 20.80 g oxalic acid dihydrate (0.165 mol) in 500 ml water is slowly added, forming a white precipitate. The solid is filtered off, washed several times with water, and dried at 120 °C, yielding 27.01 g $La_2(C_2O_4)_3{\cdot}H_2O$ (0.048 mol) as white powder. The oxalate is fired in a porcelain crucible in a muffle furnace with a ramp of RT-900 °C for 12 h, held at 900 °C for 12 h, and cooled in a desiccator above KOH. Finally, 15.77 g La_2O_3 (0.048 mol) are obtained as white powder.

In a similar way, Y_2O_3, Pr_6O_{11}, Nd_2O_3, and Sm_2O_3 are prepared. In case of CeO_2, commercial $Ce(NO_3)_3{\cdot}6H_2O$ is used for the preparation of $Ce_2(C_2O_4)_3{\cdot}H_2O$.

2.2.2. Rare earth oxides on γ-Al_2O_3

The γ-Al_2O_3 support is dried 16 h at 200 °C and kept dry before use. For 10% La_2O_3 loading, 18 g of γ-Al_2O_3 is impregnated with 5.32 g $La(NO_3)_3{\cdot}6H_2O$ (12.3 mmol) dissolved in 50 ml distilled water. After drying at 120 °C, the cake is powdered and calcined by a ramp of RT-900 °C for12 h and held at 900 °C for12 h in a muffle furnace. For 20% La_2O_3 content, 16 g γ-Al_2O_3 is twice successively impregnated and calcined with 5.32 g $La(NO_3)_3{\cdot}6H_2O$ (2 × 12.3 mmol), and for 50% La_2O_3 content, 10 g γ-Al_2O_3 is four times successively impregnated and calcined with each 6.65 g $La(NO_3)_3{\cdot}6H_2O$ (4 × 14.4 mmol).

The preparation of 10% oxides of Pr, Nd, Sm, Gd, Dy, Er, or Yb on γ-Al_2O_3 follows the same procedure. The loading is related to the oxides in the oxidation state 3+, irrespective of the oxidation state in the pure rare earth oxides.

2.2.3. Y_2O_3 or La_2O_3 on monoclinic or tetragonal ZrO_2

The different zirconium hydroxide precursors were calcined by a ramp of RT-700 °C for 6 h and held at 700 °C for 6 h. From $Zr(OH)_4$ monoclinic m-ZrO_2, from $Zr(OH)_4$/10% La_2O_3 stabilized tetragonal t-ZrO_2/10% La_2O_3 and from $Zr(OH)_4$/8% Y_2O_3 also stabilized tetragonal t-ZrO_2/8% Y_2O_3 are formed. In the following 18 g m-ZrO_2 or 18 g t-ZrO_2/10% La_2O_3 is impregnated with each 5.32 g $La(NO_3)_3{\cdot}6H_2O$ (12.3 mmol), or 18 g t-ZrO_2/8% Y_2O_3 is impregnated with 6.78 g $Y(NO_3)_3{\cdot}6H_2O$ (17.7 mmol) in the common way. After calcination by a ramp of RT-700 °C for 6 h and holding at 700 °C for 6 h, the three catalysts m-ZrO_2/10%La_2O_3, t-ZrO_2/19% La_2O_3, and t-ZrO_2/17.8% Y_2O_3 are obtained.

2.2.4. La_2O_3 on activated carbon

The preparation of 50% La_2O_3 on activated carbon is conducted in a 250 ml round-bottomed flask equipped with condenser, mechanical stirrer, and tempered oil bath. A mixture of 26.58 g $La(NO_3)_3{\cdot}6H_2O$ (61.4 mmol), 22.12 g urea (0.368 mol), 10 g activated carbon, and 100 ml distilled water is heated to reflux under continuous agitation for 16 h. The solids are filtered off, washed with water, and dried at 120 °C. The catalyst activation is done in a quartz tube oven by calcination under high vacuum using a ramp of RT-900 °C for 3 h and keeping at 900 °C for 3 h. After cooling under vacuum, 19.45 g of black powder is obtained.

For a loading of 20% La_2O_3, 10.63 g $La(NO_3)_3{\cdot}6H_2O$ and 16 g activated carbon and for 10% La_2O_3, 5.32 g $La(NO_3)_3{\cdot}6H_2O$ and 18 g activated carbon are used. The required amount of urea and water is not changed.

2.2.5. Rare earth mixed oxides by flash combustion synthesis

Several mixed oxides were prepared by flash combustion synthesis. The formulations are based on a complete combustion of the metal nitrates and glycine to CO_2, H_2O, N_2, and the desired mixed oxide. This means a nitrate/glycine stoichiometric ratio of 9:5 is used. In the following an example of each compound class is given. Precaution should be taken before scale-up of the given formulations, because the reaction might become too vigorous.

2.2.5.1. Rare earth aluminates. A solution of 18.76 g $Al(NO_3)_3{\cdot}9H_2O$ (0.05 mol), 21.65 g $La(NO_3)_3{\cdot}6H_2O$ (0.05 mol), and 12.51 g glycine (0.167 mol) in 25 ml water is prepared. The mixture is calcined in a porcelain dish inside of a preheated oven of 500 °C for 15 min. The mixture starts to boil and dehydrate, forming a foam, which ignites with a bright flame and vigorous gas evolution. The voluminous solid is powdered and 11.41 g gray crude product is obtained. An additional calcination step with a ramp of RT-1000 °C for 6 h and keeping at 1000 °C for 6 h yields 10.45 g $LaAlO_3$ (0.049 mol) as a fine white powder. In a similar way, $PrAlO_3$, $NdAlO_3$, and $SmAlO_3$ are obtained.

The $Y_3Al_5O_{12}$ is made from 37.51 g $Al(NO_3)_3{\cdot}9H_2O$ (0.1 mol), 22.98 g $Y(NO_3)_3{\cdot}6H_2O$ (0.06 mol), and 20.02 g glycine (0.267 mol). After calcination of 11.98 g crude product, 11.67 g $Y_3Al_5O_{12}$ (0.020 mol) is obtained as white powder.

2.2.5.2. Rare earth zirconates. For example, 24.60 g of aqueous 1.6257 mol/kg $ZrO(NO_3)_2$ solution (0.04 mol), 17.32 g $La(NO_3)_3{\cdot}6H_2O$ (0.04 mol), and 11.68 g glycine (0.156 mol) are dissolved in additional 15 ml of water. The two-step calcination procedure yields 10.82 g $La_2Zr_2O_7$ (0.019 mol) as white powder. The same synthesis is adopted to the preparation of $Pr_2Zr_2O_7$, $Nd_2Zr_2O_7$, $Sm_2Zr_2O_7$, and $Y_2Zr_2O_7$.

2.2.5.3. Rare earth titanates. Typically, 63.64 g of aqueous 0.7857 mol/kg $TiO(NO_3)_2$ solution (0.05 mol), 21.65 g $La(NO_3)_3{\cdot}6H_2O$ (0.05 mol), and 14.60 g glycine (0.194 mol) are dissolved. The two-step calcination procedure yields 11.74 g $La_2Ti_2O_7$ (0.024 mol) as white powder. The titanates $Pr_2Ti_2O_7$, $Nd_2Ti_2O_7$, $Sm_2Ti_2O_7$, and $Y_2Ti_2O_7$ are successfully prepared, too.

The required $TiO(NO_3)_2$ solution was prepared by hydrolysis of $TiCl_4$ on ice, precipitation of $TiO_2{\cdot}xH_2O$ with NH_3, washing the precipitate with distilled water until free of chloride, and dissolving the wet cake in 65% HNO_3.

2.3. Catalyst characterization

The X-ray powder diffraction patterns were recorded on a Siemens D5000 of 217.5 mm goniometer radius. A copper anode with Cu Kα1 (154.0598 pm), Cu Kα2 (154.4426 pm), and nickel filter was used as X-ray source. Measurements were done in the 2Θ range 3–90° with 0.02° step width and 1 s data acquisition.

Lattice constants were determined by Cu Kα2 stripping and additional fitting of the sample height displacement by the standard least square method.

Crystal size d was determined by the Scherrer method with the full-width in half-height w assuming a Lorentz peak shape following equation:

$$d = \frac{0.9 \cdot \lambda}{(w - w_0) \cdot \cos\Theta} \quad (1)$$

The line width w_0 was determined to be 0.0693°·cos Θ. The lattice strain could not be fitted, due to the too high experimental and systematic errors. The crystallite sizes are based upon the average of all d values calculated from reflections with $2\Theta > 30.00°$ and a peak area >2500 counts.

The nitrogen adsorption isotherms were measured on a Micromeritics ASAP 2010 at 77 K. The BET surface area was calculated for the partial pressure range p/p_0 of 0.05–0.25, the micropores for 0.2–2 nm diameter and the mesopores for 2–100 nm diameter using the BJH method.

The TG analysis was performed on a Netzsch STA 409C in the range 20–1100 °C and 2 °C/min temperature ramp in dry air.

The TPD analysis was conducted on a Carlo Erba TPDRO 1100 Series Thermo Finnigan. Samples were degassed at 500 °C in a he-

lium atmosphere and loaded at 30 °C with CO_2. Desorption was performed in the range 30–900 °C with helium as carrier gas and thermal conductivity detection (TCD).

2.4. Transesterification procedure

Transesterifications were conducted in 75 ml steel autoclaves equipped with glass inlet, pressure gauge of 0.25 bar accuracy, internal thermocouple, and 5 × 20 mm magnetic stirring bars at 500 rpm. A Horst 325 W heating mantle regulated with Eurotherm 91e controller was used for temperature regulation with an accuracy of ±5 °C.

In a typical run, 12.5 g oil, 12.5 g methanol, and 1.25 g of catalyst are used. This means 50% methanol and a triglyceride/methanol ratio of 1:27.5 for rapeseed oil and of 1:26.4 for both crude and refined palm oil is used. In addition, 16.25 g rapeseed oil, 8.75 g methanol, and 1.63 g catalyst according to 35% methanol and 1:14.8 stoichiometry and 20 g rapeseed oil, 5 g methanol, and 2 g catalyst according to 20% methanol and 1:6.9 stoichiometry were used, too. This means that always 10% of catalyst related to the oil amount is used.

Typically, the temperature is raised to 150 °C in 15 min, to 200 °C in 25 min, and to 250 °C in 40 min. The reaction time is set zero, when the desired temperature is reached by ±5 °C accuracy. After finishing 2 h of reaction time, the autoclave is quenched in ice. The resulting two liquid phase mixture is diluted with 30 ml MTBE, the catalyst separated by centrifugation, and the product mixture analyzed by GC.

The initial pressures obtained with rapeseed oil are summarized in Table 1.

With 50% methanol and 225 °C, 52 bar are reached, and at 250 °C, even 78 bar are measured. The progress of the transesterification can be followed by a pressure drop. For example, with 50% methanol and 250 °C the pressure ends up at 62 bar for full conversion.

2.5. Product analysis

The fatty acid composition of the triglycerides was determined by GC of the methylesters on a Hewlett Packard 6890 GC equipped with a 50 m, 0.25 mm, 0.25 μm carbowax-coated capillary column from CS Chromatographie using 120 °C, 2 min iso, 120–230 °C, 5 °C/min, 230 °C, 20 min iso temperature program. Methylheptadecanoate was used as internal standard for calibration.

The transesterification product analysis was carried out on a Hewlett Packard 6890 GC equipped with cool on-column injector system, a 12 m, 0.32 mm, 0.1 μm HT5-coated capillary column from SGE using 60 °C, 1 min iso, 60–350 °C, 10 °C/min, 350 °C, 20 min iso temperature program. Tricaprin was used as internal standard for calibration. Samples were silylated using BSTFA and pyridine as silylating reagents. Excess methanol was removed in vacuum, 25 μl of dry sample was dissolved in 250 μl MTBE and silylated with 100 μl pyridine and 50 μl BSTFA in the sealed GC glass for 30 min at 70 °C. After cooling, samples were made up with MTBE to 1.6 ml and directed to GC analysis [111]. The accuracy of product composition was ±0.5%.

Table 1
Initial pressure conditions for the transesterification of crude rapeseed oil.

Temperature (°C)	20% methanol (bar)	35% methanol (bar)	50% methanol (bar)
50	9	10	10.75
175	12	18	21
200	18.5	28.5	33

2.6. Calculation of the methylester and glycerol yields and selectivities

The transesterification of triglycerides is a three-step consecutive reaction as shown in Fig. 1.

Starting from the triglycerides TG via the intermediate 1,2- and 1,3-diglycerides DG and 1- and 2-monoglycerides MG, finally glycerol G is formed. In any of the three consecutive steps an equivalent of FAME is formed. The complete liberation of the glycerol requires very high conversions, because only in the last step the glycerol is formed, while only 1/3 of the FAME comes out.

For the calculation of the yields Y and selectivities S the total amounts of fatty acids and glycerol in both, free and bound form, must be determined by GC analysis. The total amount of free and bound fatty acids n_{FBFA} is given by:

$$n_{FBFA} = 3n_{TG} + 2n_{DG} + n_{MG} + n_{FAME} + n_{FFA} \quad (2)$$

In a similar way, the total amount of free and bound glycerol n_{FBG} is given by:

$$n_{FBG} = n_{TG} + n_{DG} + n_{MG} + n_{G} \quad (3)$$

The stoichiometric ratio ν_{FBFA} between the free and bound fatty acids n_{FBFA} and the free and bound glycerol n_{FBG} must be constant and is expressed by:

$$\nu_{FBFA} = \frac{n_{FBFA}}{n_{FBG}} \quad (4)$$

In idealized triglycerides the stochiometric ratio should be 3. In real fats and oils deviations from the ideal ratio are observed, due to the formation of free fatty acids and partial glycerol loss in crude oils and fats and excess diglycerides and monoglycerides in refined fats and oils.

The conversion X is related to the number of cleaved glycerol ester groups according to:

$$X = \frac{n_{FAME} + n_{FFA}}{3n_{TG} + 2n_{DG} + n_{MG} + n_{FAME} + n_{FFA}} \quad (5)$$

According to this definition, the conversion might be $X > 0$, if the oil contains free fatty acids.

In the following two different product selectivities are discussed. The FAME selectivity S_{FAME} is reduced due to the FFA formation, while the glycerol selectivity S_G is reduced due the accumulation of diglycerides and monoglycerides as intermediates. Based on this, the selectivities are calculated by:

$$S_{FAME} = \frac{n_{FAME}}{n_{FAME} + n_{FFA}} \quad (6)$$

$$S_G = 1 - \frac{(\nu_{FBFA} - 3)n_{TG} + (\nu_{FBFA} - 2)n_{DG} + (\nu_{FBFA} - 1)n_{MG}}{n_{FAME} + n_{FFA}} \quad (7)$$

The FAME yield Y_{FAME} and glycerol yield Y_G are defined as product of the conversion X and the selectivities S_{FAME} or S_G by Eqs. (7) and (8).

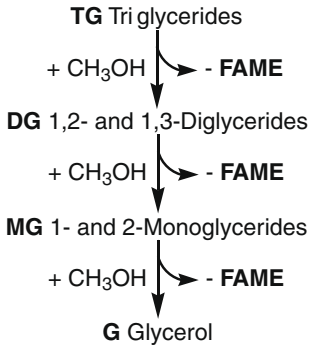

Fig. 1. Schematic transesterification of triglycerides with methanol.

$$Y_{FAME} = \frac{n_{FAME}}{3n_{TG} + 2n_{DG} + n_{MG} + n_{FAME} + n_{FFA}} \quad (8)$$

$$Y_G = 1 - \frac{v_{FBFA}(n_{TG} + n_{DG} + n_{MG})}{3n_{TG} + 2n_{DG} + n_{MG} + n_{FAME} + n_{FFA}} \quad (9)$$

In this manner, the glycerol yield Y_G and selectivity S_G are determined indirectly via the total stoichiometry. The direct quantification of glycerol causes problems, due to the strong adsorption on the high catalyst surfaces.

2.7. Calculation of the specific surface activity

Due to the low surface area of the investigated catalysts, the BET surface area could not be measured with sufficient accuracy. Therefore, the specific catalyst surface area A was calculated using the X-ray density ρ and the crystal size d obtained by the Scherrer method Eq. (1) as given by:

$$A = \frac{6}{\rho \cdot d} \quad (10)$$

The rate constant k is based on the assumption of a pseudo-first order reaction kinetics and calculated with aid of the reaction time t and the conversion X of Eq. (5) as given by:

$$k = -\frac{\ln(1 - X)}{t} - k_0 \quad (11)$$

The non-catalytic rate constant k_0 was determined to be 0.0244 h^{-1}. Finally, the specific surface activity is related to the catalyst mass $m_{Catalyst}$ and the molar amount of ester groups in the oil n_{Ester} as given by:

$$\text{Activity} = \frac{k \cdot n_{Ester}}{m_{Catalyst} \cdot A} \quad (12)$$

As standard conditions, 2 h reaction time, 12.5 g refined palm oil corresponding to n_{Ester} = 44.182 mmol, and $m_{Catalyst}$ = 1.25 g were used for the calculations.

3. Results and discussion

3.1. Oil characterization

The fatty acid mass distribution of rapeseed oil, crude and refined palm oil is listed in Table 2.

The rapeseed oil is mainly assembled of oleic acid 18:1, while for crude and refined palm oil palmitic acid 16:0 is predominant.

The acylglycerol composition of the three different oils is summarized in Table 3.

The refined palm oil is free of FFA, rapeseed oil has a low content of 0.7% FFA, and crude palm oil has a high content of 5.0% FFA. This refers to an acid value of 10.5 mg KOH/g oil.

3.2. Blank experiments

For rapeseed oil and 50% methanol the obtained product composition is given by Fig. 2.

As expected, an increase in the temperature leads to a fast increase in the transesterification rate. At 150 °C 0.2%, at 200 °C 4.2%, and at 250 °C 40.4% FAME yield are obtained. In addition, an increase in the methanol content surprisingly leads to a slightly decreasing FAME yield. For example, at 200 °C with 20% methanol 8.8% FAME, and with 50% methanol only 4.2% FAME are obtained. This might be explained by the autocatalytic action of the small FFA content of 0.7% in the rapeseed oil. These findings are in good agreement with reports for soybean oil and 44% methanol. After 2 h at 220 °C and 55 bar 26% FAME yield and at 235 °C and 62 bar 79% FAME yield was reported [112]. Another group published for rapeseed oil, 61% methanol, 1 h at 270 °C, and 200 bar 36% FAME yield and at 300 °C and same pressure 73% FAME yield [113].

Furthermore, the formed FFA content is also increasing in the order 0.2% at 150 °C, 1.0% at 200 °C, and 2.6% at 250 °C. This might be caused by saponification of the triglycerides by small amounts of water in the methanol and oil. This is an important observation, because basic transesterification catalysts are known to be unstable towards FFA. Therefore, not only a small FFA content but also a low water content in the feedstock is of importance.

Hence, to judge the following heterogeneously catalyzed transesterifications, the non-catalytic transesterification can be neglected at temperatures of 200 °C and lower.

Table 3
Acylglycerol composition, free fatty acid content, and acid value of different oils.

	Rapeseed oil	Crude palm oil	Refined palm oil
Triglycerides (wt.%)	98.2	87.8	91.0
Diglycerides (wt.%)	1.2	6.7	9.0
Monoglycerides (wt.%)	0	0.5	0
Free fatty acids (wt.%)	0.7	5.0	0
Acid value (mg KOH/g oil)	1.3	10.5	0

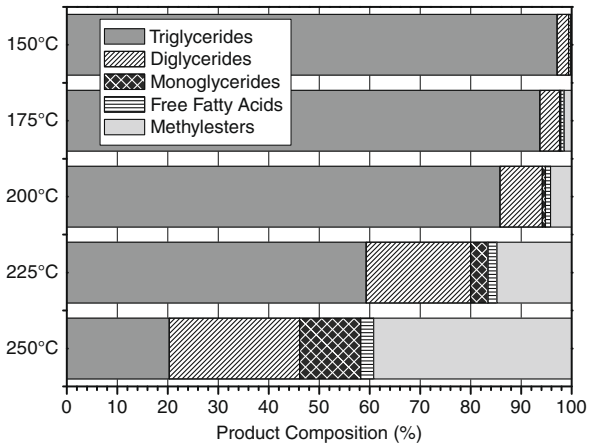

Fig. 2. Effect of the temperature on the non-catalytic transesterification using rapeseed oil and 50% methanol as feed.

3.3. Activity of different rare earth oxides with crude and refined palm oil

Starting from the rare earth oxalates, the rare earth oxides of La to Sm and Y were made by 12 h calcination at 900 °C. The XRD results are shown in Fig. 3.

Table 2
Fatty acid composition of the vegetable oils used in this work.

Fatty acid	12:0	14:0	16:0	16:1	18:0	18:1	18:2	18:3	20:0	20:1	22:0	22:1	24:0	24:1
Rapeseed oil	–	0.4	4.4	0.4	1.5	61.6	19.7	9.1	0.4	1.2	0.4	0.5	0.2	0.2
Crude palm oil	0.1	1.2	48.4	0.4	4.6	36.2	8.2	0.2	0.4	0.3	–	–	–	–
Refined palm oil	0.4	1.2	44.7	0.5	4.1	38.7	9.7	0.1	0.4	0.2	–	–	–	–

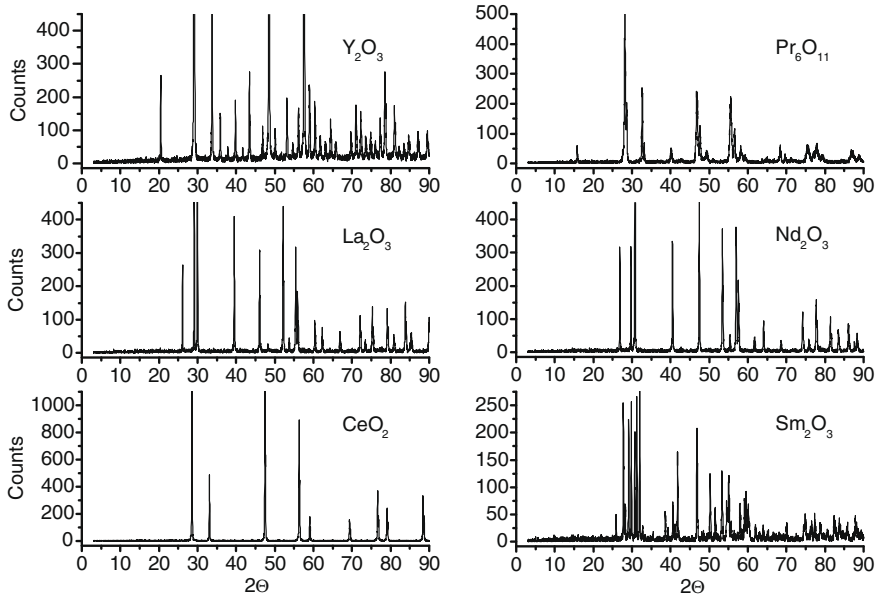

Fig. 3. X-ray powder diffraction patterns of different rare earth oxides.

The X-ray powder diffraction patterns match the well-known rare earth oxide structures [114], which are represented by the Mn_2O_3 type for Y_2O_3, the α-La_2O_3 type for La_2O_3 and Nd_2O_3, the CaF_2 type for CeO_2, a distorted CaF_2 super structure with ordered oxygen vacancies for Pr_6O_{11} and finally the β-La_2O_3 type for Sm_2O_3.

All oxides are of high crystallinity, and the BET surface area could not be determined accurately due to values of <5 m^2/g. Therefore, an enhancement of the specific catalyst surface area was of interest. For this purpose, thermogravimetric measurements to determine the minimum calcination temperature necessary to obtain the pure oxides and minimize sintering effects were conducted. A typical TGA starting from $La_2(C_2O_4)_3{\cdot}H_2O$ is shown in Fig. 4.

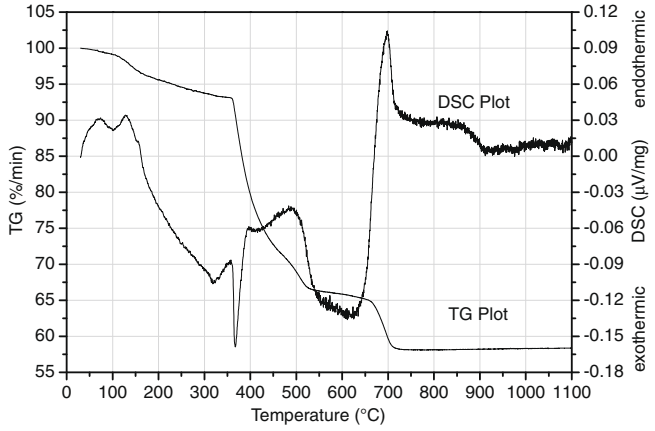

Fig. 4. Thermogravimetric plot of lanthanum oxalate $La_2(C_2O_4)_3{\cdot}H_2O$.

The decomposition of $La_2(C_2O_4)_3{\cdot}H_2O$ takes place in several consecutive steps of 30–180 °C dehydration, 180–460 °C decomposition of the oxalate into the instable intermediate $La_2O(CO_3)_2$, 460–550 °C CO_2 release and transformation to $La_2O_2(CO_3)$ as an isolable intermediate, and 550–750 °C final CO_2 release and formation of the desired La_2O_3. The differential scanning calorimetry DSC indicates that the decomposition of the oxalate is maximum exothermic at 367 °C, while the decomposition of the $La_2O(CO_3)_2$ is endothermic at 487 °C and of $La_2O_2(CO_3)$ is endothermic at 697 °C.

The TGA results of all investigated rare earth oxalates are summarized in Table 4.

With decreasing cation radius and basicity the $RE_2O_2(CO_3)$ intermediate is no longer apparent beyond Nd. The behavior of $Ce_2(C_2O_4)_3{\cdot}H_2O$ is very different, which only consists of dehydration from 30 to 210 °C and direct formation of CeO_2 from 210 to 350 °C with a high exothermic peak at 281 °C. In the series La to Sm and Y, the calcination temperature necessary to obtain the pure oxides is decreasing slightly from approximately 750–650 °C. Furthermore, transformation is kinetically hindered, and the phase transition temperature is substantially lowered for infinite reaction time. These tendencies are in accordance with the reviewed literature [115,116].

However, for the preparation of pure La_2O_3 practically at least 850 °C is necessary, to convert the remaining $La_2O_2(CO_3)$ to the oxide in a reasonable period of time.

Table 4
Thermogravimetric analysis of different rare earth oxalates.

Compound	$La_2(C_2O_4)_3$		$Ce_2(C_2O_4)_3$		$Pr_2(C_2O_4)_3$		$Nd_2(C_2O_4)_3$		$Sm_2(C_2O_4)_3$		$Y_2(C_2O_4)_3$	
	(%)	(°C)	(%)	(°C)	(%)	(°C)	(%)	(°C)	(%)	(°C)	(%)	(°C)
$RE_2(C_2O_4)_3{\cdot}xH_2O$	100.00	30	100.00	30	100.00	30	100.00	30	100.00	30	100.00	30
$RE_2(C_2O_4)_3$	95.60	203	96.87	210	96.51	280	90.11	300	90.03	285	96.93	180
$RE_2O(CO_3)_2$	71.28	470	–	–	73.32	439	72.82	437	–	–	–	–
$RE_2O_2(CO_3)$	66.11	570	–	–	66.60	496	61.17	551	60.01	580	55.37	549
REO	58.33	750	62.24	350	60.87	608	55.91	664	56.86	650	48.63	681
Loss on ignition	58.13	1000	60.43	1000	59.82	1000	55.06	1000	56.50	1000	47.86	1000

A comparison of the catalytic performance of different at 900 °C calcined rare earth oxides in the transesterification of refined and crude palm is shown in Fig. 5.

When 50% methanol is used at 200 °C, the methylester yield is decreasing in the order La to Sm and Y for refined and crude palm oil, respectively. This can be explained by the same decreasing order of the cation radius and of the basicity. This trend leads to an activity optimum for La_2O_3, which converts refined palm oil with 90.6% FAME and 84.7% glycerol yield, while crude palm oil even makes 97.2% FAME and 94.2% glycerol yield. Surprisingly, the presence of 5.0% FFA in crude palm oil always leads to methylester yields exceeding the values of refined palm oil. This does not match our expectations, because in the presence of FFA the basic surface activity should be reduced. However, the formation of basic soaps might cause some partition of homogeneous catalysis. Deviating from the other rare earth oxides, CeO_2 is of higher oxidation state, shows much less basicity and almost no catalytic activity.

For comparison, the non-catalytic conversion of refined palm oil yields 3.9% FAME and of crude palm oil 9.5% FAME. Again the presence of FFA accelerates the auto catalytic reaction rate.

These results confirm the well-known fact that in the lanthanide series from La to Lu the decreasing ion radius causes a diminishing basicity and catalytic activity of the corresponding oxides [117]. In addition, the light rare earth element yttrium is similar to holmium in terms of ionic radius and basicity. Therefore, the rare earth elements offer the unique opportunity, to control the base strength and to study the specific catalyst optimization.

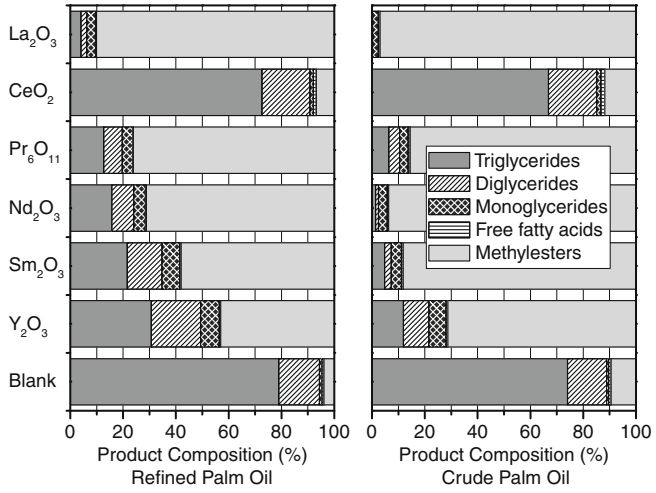

Fig. 5. Product composition using crude or refined palm oil and 50% methanol as feed in presence of different rare earth oxides at 200 °C.

3.4. Optimization of the reaction conditions for lanthanum oxide with rapeseed oil

For the most active La_2O_3, which was calcined at 900 °C, an optimization study with rapeseed oil was conducted in order to investigate the influence of the temperature and the methanol amount on the product scope. The results are shown in Fig. 6.

According to the expectations both, a rising methanol content and temperature, result in an increased rapeseed oil conversion. Starting from the lower limits of 150 °C and 20% methanol only 20.1% FAME and 7.4% glycerol yield are obtained. At the upper limits of 200 °C and 50% methanol a product comprising 0.3% diglycerides, 2.3% monoglycerides, 0.3% FFA, and 97.1% FAME is obtained. Hence, the composition already presents the thermodynamic equilibrium under these conditions. That means 97.5% FAME yield at 99.7% selectivity and 93.8% glycerol yield at 95.9% selectivity are formed.

3.5. Activity of different rare earth oxides on γ-Al_2O_3

The surface properties of the rare earth oxides starting from the oxalates can not be significantly improved by lowering the calcination temperature and reduction in sintering effects. The industrial application of heterogeneous catalysts requires easy and reproducible preparation techniques. Therefore, different catalyst supports such as Al_2O_3, TiO_2, ZrO_2, Fe_2O_3, and SnO_2 were screened to reduce the amount of active compound necessary. An improvement of the surface properties was expected. In the course of successive loading by impregnation with the corresponding rare earth nitrates followed by activation at 900 °C, any oxidic support material causes the formation of surface mixed oxide phases. This leads to a reduced surface basicity and catalyst activity.

However, the decision was made to investigate γ-Al_2O_3 as support in more detail. For Gd to Lu and Y cubic garnets of the composition $RE_3Al_5O_{12}$, for La to Dy and Y perovskites of the general formula $REAlO_3$, and for Sm to Lu and Y mixed oxides of the $RE_4Al_2O_9$ type are known to be stable [118]. For the preparation of γ-Al_2O_3 supported rare earth oxides, the phases with the highest aluminum content are expected to be formed. These are the perovskites for La to Eu and the garnets for Gd to Lu and Y.

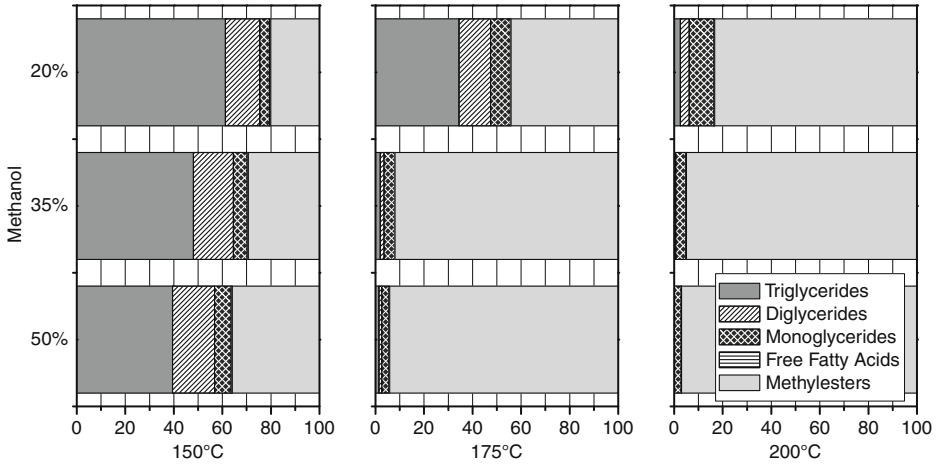

Fig. 6. Effect of the temperature and methanol content on the product composition using rapeseed oil as feed in the presence of La_2O_3.

A whole series of 10% rare earth oxide on γ-Al_2O_3 catalysts was prepared by calcination at 900 °C. The results using rapeseed oil as feed are summarized in Fig. 7.

The results obtained with rapeseed oil and 50% methanol at 200 °C show that the trivalent rare earth oxides on γ-Al_2O_3 exhibit universal activity in the transesterification. The scope of products ranges between a minimum of 45.9% FAME and 32.3% glycerol yield for 10% La_2O_3 loaded on γ-Al_2O_3 and a maximum of 71.2% FAME and 56.6% glycerol yield for 10% Nd_2O_3 loading.

As an exception, cerium is only partially stabilized as trivalent $CeAlO_3$ perovskite. Most of the cerium forms a separate tetravalent CeO_2 phase which is catalytically inactive as shown in Fig. 4. For cerium this effect is leading to a smaller catalytic activity in comparison with the other rare earth elements. For praseodymium a complete stabilization as $PrAlO_3$ perovskite takes place.

These results are contrary to a publication [74], which claims an excellent activity for a catalyst made of 9% Eu_2O_3 on γ-Al_2O_3 prepared by impregnation of pseudoboehmite AlO(OH) with $Eu(NO_3)_3$, followed by activation at 900 °C. In case of the transesterification of soybean oil with methanol in 1:6 stoichiometry, 10% of catalyst related to the oil, in 8 h at 70 °C 63.3% conversion is reported.

However, in practice a catalyst containing 10% Eu_2O_3 prepared according to the authors' guidelines was used for the transesterification of rapeseed oil at standard conditions of 50% methanol and 200 °C. Only 36.3% FAME yield and 27.4% glycerol yield was achieved as shown in Fig. 7. Anyway, europium is one of the rarest and most expensive lanthanide elements and features no realistic interest for an industrial application.

In summary, supported rare earth oxide catalysts on γ-Al_2O_3 always lead to the formation of surface aluminates, which are of much lower activity than the corresponding pure rare earth oxides. However, a universal activity of rare earth oxides supported on γ-Al_2O_3 is found. As an exception, cerium oxide is less active. Therefore, the much cheaper non-separated oxides can be used, which are traded as Ce depleted La to Sm light rare earth fraction and the Eu depleted Eu to Lu heavy rare earth fraction, which also might contain Y. Another advantage of supported rare earth catalysts is the reduction of the required amount of active compound and the catalyst preparation costs. In addition, the rare earth oxides like La_2O_3 are known to be sensitive towards H_2O and CO_2, which result in the formation of compounds such as $La(OH)_3$, $LaOH(CO_3)$, and $La_2O_2(CO_3)$. Finally, mixed oxides are more resistant towards FFA traces in the feedstock. This effect, for example, is advantageously applied to the IFP catalyst system [41,42]. As active compound ZnO is used, which is of high activity but poor resistance towards FFA traces due to zinc soap formation. This undesired effect was overcome by the use of γ-Al_2O_3 as support and the formation of the stable spinel phase $ZnAl_2O_4$ as active catalyst.

In case of the light rare earth oxides supported on γ-Al_2O_3 catalysts, the influence of the reaction temperature on the transesterification of rapeseed oil with 50% methanol was tested in an extensive series of experiments summarized in Fig. 8.

The results of the blank tests and the pure γ-Al_2O_3 carrier are shown as well. The comparison reveals that the support is of small catalytic activity. As already explained, the loading of cerium oxide gives a smaller increase in conversion with respect to the other rare earth oxides. The elements La, Pr, Nd, and Y are more active, typically making 9% FAME and 2% glycerol yield at 150 °C. However, at elevated temperature of 250 °C, a tremendous acceleration of the reaction rate takes place, leading to high conversions and typically 96% FAME and 92% glycerol yield. More in particular, 10% Pr_2O_3 on γ-Al_2O_3 leads to the top result of 96.8% FAME and 92.6% glycerol yield. The product comprises 0.4% diglycerides, 2.7% monoglycerides, 0.5% FFA, and 96.4% FAME. Hence, almost the thermodynamic equilibrium composition is reached.

Finally, the catalyst preparation of La_2O_3 on γ-Al_2O_3 was optimized. Different loadings of La_2O_3 could be achieved by subsequent impregnation of $La(NO_3)_3$ and calcination at 900 °C. The changes of the XRD structure are depicted in Fig. 9.

The γ-Al_2O_3 is of poor crystallinity and only broad reflections are observed. Already for the lowest loading of 10% La_2O_3, the formation of the $LaAlO_3$ perovskite phase is resolved by the X-ray powder diffraction pattern. An increasing La_2O_3 content leads to the formation of low dispersed and high crystalline $LaAlO_3$. For the highest loading of 50% La_2O_3, almost a complete conversion of the γ-Al_2O_3 has taken place. For the purpose of comparison phase pure $LaAlO_3$ of nominal 76.2% La_2O_3 content is shown, which was aberrantly prepared by flash combustion synthesis. Despite the different preparation methods, the peak broadening and crystallinity is comparable with the catalysts supported on γ-Al_2O_3.

The structural changes are accompanied by a significant loss of the BET surface area. The results are summarized in Table 5.

The γ-Al_2O_3 is a mesoporous material of 120.8 m^2/g BET surface area with a high BJH mesopore volume of 0.744 $cm^3\ g^{-1}$ and an average pore diameter of 23.8 nm. Increasing loading of La_2O_3 leads to a continuous loss of surface to finally 26.7 m^2/g BET surface area, 0.225 $cm^3\ g^{-1}$ mesopore volume, and 30.1 nm average pore diameter for 50% La_2O_3 loading. The flash combustion synthesis of $LaAlO_3$ results in a material of 14.2 m^2/g BET surface area,

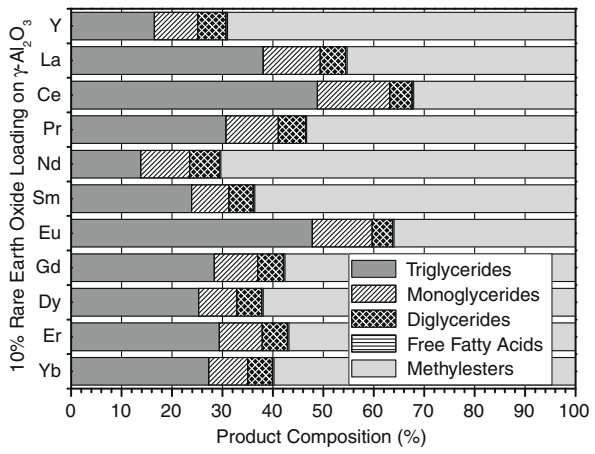

Fig. 7. Effect of 10% loading of different rare earth oxides on γ-Al_2O_3 on the methylester yield using rapeseed oil and 50% methanol as feed at 200 °C.

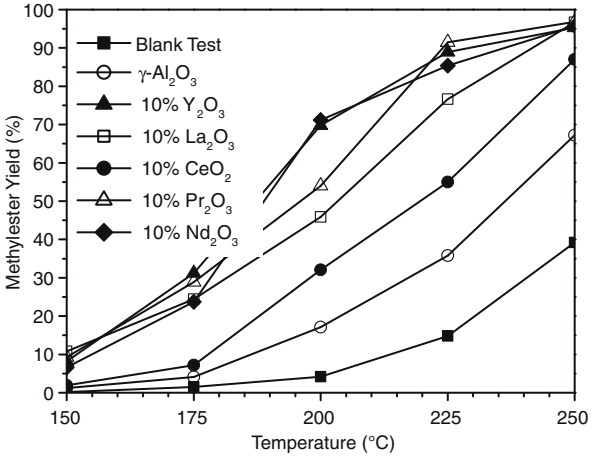

Fig. 8. Effect of 10% loading of different rare earth oxides on γ-Al_2O_3 and reaction temperature on the methylester yield using rapeseed oil and 50% methanol as feed.

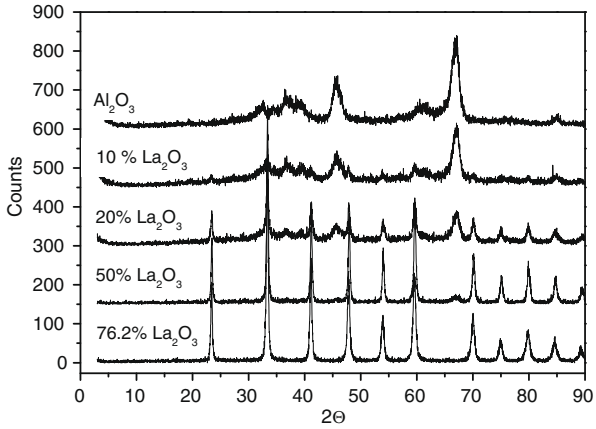

Fig. 9. Effect of the La_2O_3 loading on γ-Al_2O_3 on the X-ray powder diffraction patterns.

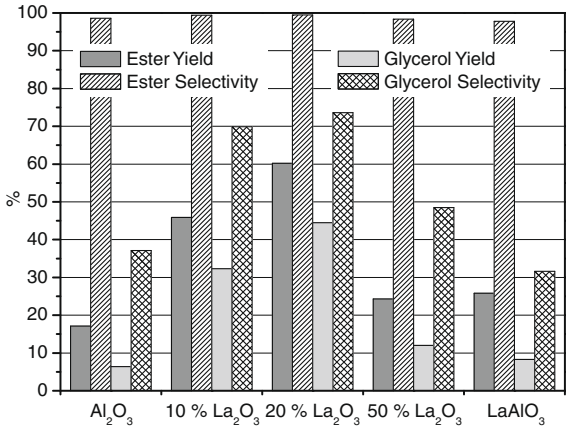

Fig. 10. Effect of the La_2O_3 content loaded on γ-Al_2O_3 upon the methylester and glycerol yields and selectivities using rapeseed oil and 50% methanol as feed at 200 °C.

0.038 $cm^3\ g^{-1}$ mesopore volume, and 6.4 nm average pore diameter. Especially the small pore volume and diameter is much different to the on γ-Al_2O_3-supported catalysts.

The results of the catalytic tests using the described lanthanum aluminates with rapeseed oil and 50% methanol at 200 °C are shown in Fig. 10.

The activity culminates at 20% La_2O_3 with 60.2% FAME yield at 99.5% selectivity and 44.5% glycerol yield at 73.6% selectivity. The maximum is caused by two opposite effects. On the one hand the active material is increased, but on the other hand the accessible surface is decreased.

Finally, the minimum temperature to achieve the complete decomposition of $La(NO_3)_3$ into La_2O_3 was determined by TGA. The limiting process is the decomposition of the oxynitrate LaO(NO_3) in the last step which requires a minimum of 700 °C calcination temperature. Therefore, a further improvement of the investigated catalysts could be achieved by reduction in the activation temperature from 900 °C to 700 °C, thereby minimizing sintering effects. In case of the heavier rare earth elements, a continuous lowering of the required calcination temperature is expected.

3.6. Activity of La_2O_3 on monoclinic or tetragonal ZrO_2

At room temperature zirconium oxide ZrO_2 can be obtained either in the monoclinic or in the tetragonal modification. In the ideal crystalline solid state only monoclinic ZrO_2 is thermodynamically stable. However, the structure of the $Zr(OH)_4$ precursor, lattice strains, and the crystallite size can stabilize the tetragonal ZrO_2 modification. Below a critical crystallite size tetragonal ZrO_2 becomes metastable [119,120]. Therefore, calcination at high temperature and sintering always results in formation of the monoclinic ZrO_2 phase. For the application as catalyst the tetragonal modification of ZrO_2 is preferred due to higher BET surface areas. A reliable method for the stabilization of tetragonal ZrO_2 is the addition of dopants like Y_2O_3 or La_2O_3.

Starting from different zirconium hydroxides $Zr(OH)_4$, the three carriers monoclinic ZrO_2, 8% Y_2O_3 stabilized tetragonal ZrO_2, and 10% La_2O_3 stabilized tetragonal ZrO_2 were obtained by calcination at 700 °C. The X-ray powder diffraction patterns of the $Zr(OH)_4$ precursors are shown on the top of Fig. 11.

The monoclinic ZrO_2 carrier was loaded with 10% La_2O_3, and the final catalyst structure is shown at the bottom of Fig. 11. Interestingly, the La_2O_3 dopant does not lead to the transformation into tetragonal ZrO_2. No free La_2O_3 can be seen and the La_2O_3 must be either high dispersed on the surface or incorporated in the surface ZrO_2 lattice by solid state diffusion. The catalyst reflects exactly the powder XRD pattern of the carrier ZrO_2.

In the same manner, 10% La_2O_3 stabilized tetragonal ZrO_2 was loaded with further 10% La_2O_3, leading to 19% La_2O_3 in total and tetragonal ZrO_2 as shown in Fig. 11. Again no La_2O_3 phase is apparent and a slight broadening of the (1 1 1) spacing from 296.4 pm to 296.8 pm takes place by incorporation of additional La_2O_3 in the ZrO_2 lattice.

Finally, 8% Y_2O_3 stabilized tetragonal ZrO_2 was loaded with additional 10% Y_2O_3, making 17.2% dopant in total. The (1 1 1) spacing is enlarged from 296.4 pm to 296.9 pm. As expected, tetragonal ZrO_2 is in comparison with monoclinic ZrO_2 of smaller crystallite size and has a higher catalyst surface area.

The performance of the three carrier materials and the thereof prepared catalysts using refined palm oil and 50% methanol at 200 °C is compared in Fig. 12.

In general, the loading of the different supports with either Y_2O_3 or La_2O_3 gives a significant acceleration of the transesterification reaction rate. The activity of the ZrO_2 carriers is small and ranging between 6.0% FAME yield for monoclinic m-ZrO_2, 10.8% for 8% Y_2O_3 stabilized tetragonal t-ZrO_2, and 13.6% for 10% La_2O_3 stabilized tetragonal t-ZrO_2. For comparison, the blank test gave 3.9% FAME yield. The loading with 17.2% Y_2O_3 on t-ZrO_2 leads to an intermediate activity of 42.0% FAME yield. However, the loading of 10%

Table 5
Effect of the La_2O_3 loading on γ-Al_2O_3 on the BET surface area, micropore surface area, and BJH mesopore surface area.

	γ-Al_2O_3	10% La_2O_3	20% La_2O_3	50% La_2O_3	$LaAlO_3$
BET Surface area (m^2/g)	120.8	81.1	60.6	26.7	14.5
Micropore surface area (m^2/g)	11.2	7.5	7.5	2.7	0.7
Micropore volume (cm^3/g)	0.005	0.003	0.003	0.001	0
Mesopore surface area (m^2/g)	124.9	94.9	70.4	30.0	24.0
Mesopore volume (cm^3/g)	0.744	0.597	0.507	0.225	0.038
Average pore diameter (nm)	23.8	25.1	28.8	30.1	6.4
Maximum pore diameter (nm)	30.2	27.8	34.8	34.0	5.2

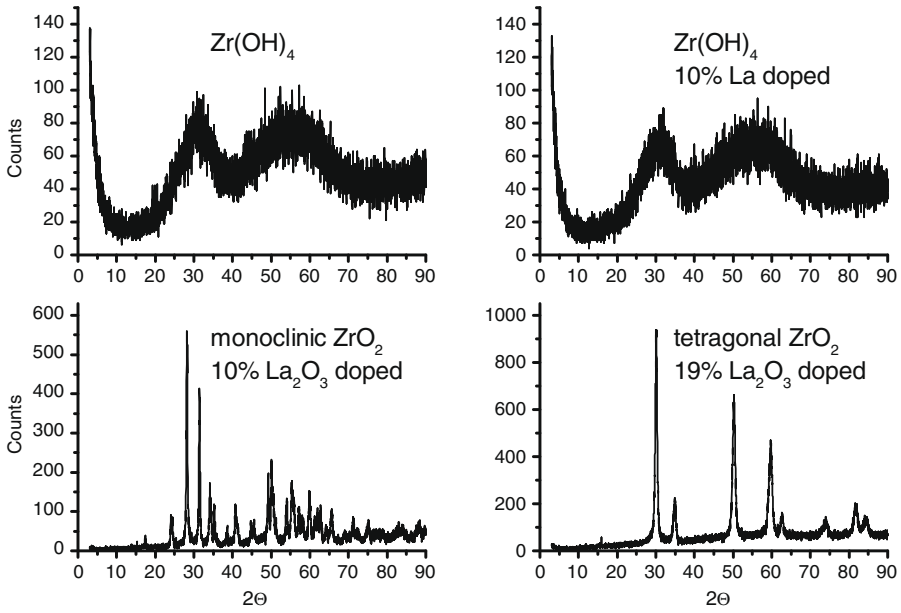

Fig. 11. X-ray powder diffraction patterns of different $Zr(OH)_4$ precursors and thereof prepared 10% La_2O_3 on ZrO_2 catalysts.

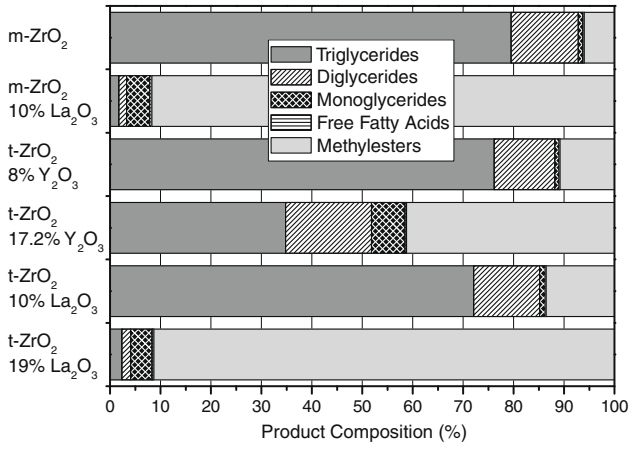

Fig. 12. Product composition using refined palm oil and 50% methanol as feed in presence of ZrO_2 or Y_2O_3 and La_2O_3-doped ZrO_2 at 200 °C.

La_2O_3 on m-ZrO_2 shows its real merits , providing 92.5% FAME yield at 99.5% selectivity and 85.2% glycerol yield at 91.7% selectivity. In addition, the 19% La_2O_3-doped t-ZrO_2 is also very good, yielding 92.0% FAME and 85.1% glycerol.

3.7. Activity of different rare earth aluminates, titanates, and zirconates

Flash combustion synthesis [121,122] is a reasonable method for the preparation of a library of stoichiometric mixed oxides as heterogeneous catalysts in a short time and with high purity. The term flash combustion synthesis means the preparation of metal oxides starting from a concentrated aqueous solution of the corresponding metal nitrates as oxidants and organic reducing agents. Such a solution is calcined at typically 500 °C, forming a melt, which finally burns in a few seconds to the desired oxide and only gaseous products such as H_2O, CO_2, and N_2. Typical reducing agents are citric acid, urea, or glycine. The product properties can be influenced by the heat of combustion, the amount of evolved gases, and the complexing properties of the organic reduction agent. The low crystallinity of the voluminous, finely powdered crude product can be influenced by an additional calcination step.

This methodology was successfully applied to the preparation of different aluminates, titanates, and zirconates of La to Sm and Y where glycine was used as the reducing agent.

The X-ray diffraction patterns of the prepared rare earth aluminates are illustrated in Fig. 13.

The lattice constants of $LaAlO_3$ to $SmAlO_3$ could not be determined, due to the small distortions of the cubic perovskite unit cell. In particular, for the perovskites of La to Nd a trigonal cell with two perovskite subunits and for Sm to Lu an orthorhombic unit cell with four perovskite subunits are reported [123,124]. Due to this reason close-neighboured reflections occur. Only the (1 0 0) and (2 0 0) reflections are not superimposed reflections, which are suitable for particle size calculations following Eq. (1). The average crystallite diameters d are for $LaAlO_3$ 26(5) nm, $PrAlO_3$ 50(9) nm, $NdAlO_3$ 75(13) nm, and $SmAlO_3$ 102(18) nm. Therefore, a clear tendency of an increasing crystallinity in the series La to Sm can be found.

The $Y_3Al_5O_{12}$ garnet is of cubic structure, and the calculated lattice constant (Table 6) is in agreement with the literature [118]. The average particle size is calculated to be 78(13) nm.

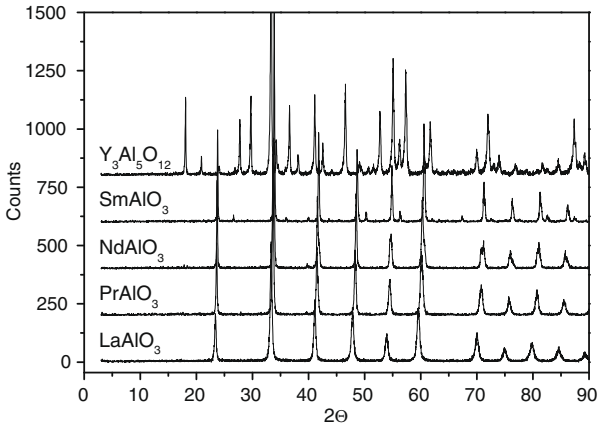

Fig. 13. X-ray powder diffraction patterns of different rare earth aluminates.

Table 6
Lattice constants, unit cell volumes, XRD-density, average crystallite size, and number of reflections used for crystallite size calculation.

Compound	a (pm)	b (pm)	c (pm)	β (°)	V (Å^3)	ρ (g/cm^3)	d (nm)	Reflections
$La_2Zr_2O_7$	1080.4(3)	–	–	–	1261(1)	6.029(5)	26(5)	8
$Pr_2Zr_2O_7$	1069.3(2)	–	–	–	1222.7(5)	6.261(3)	28(4)	7
$Nd_2Zr_2O_7$	1066.3(3)	–	–	–	1212.4(9)	6.387(5)	25(2)	7
$Sm_2Zr_2O_7$	1058.1(3)	–	–	–	1185(1)	6.674(6)	23(2)	5
$Y_2Zr_2O_7$	521.2(1)	–	–	–	141.6(1)	5.539(5)	21(1)	8
$La_2Ti_2O_7$	1302.8(2)	555.0(1)	782.4(2)	98.66(2)	559.3(3)	5.766(4)	119(15)	5
$Pr_2Ti_2O_7$	1300.45(7)	548.83(4)	771.93(9)	98.568(8)	544.8(1)	5.969(1)	199(49)	6
$Nd_2Ti_2O_7$	1299.9(3)	546.8(1)	768.7(2)	98.58(2)	540.3(4)	6.100(5)	91(24)	6
$Sm_2Ti_2O_7$	1023.7(2)	–	–	–	1072.7(7)	6.297(4)	161(42)	12
$Y_2Ti_2O_7$	1010.1(2)	–	–	–	1030.5(5)	4.970(3)	163(37)	10
$Y_3Al_5O_{12}$	1201.1(4)	–	–	–	1733(2)	4.551(5)	78(13)	9

The X-ray diffraction patterns of the prepared rare earth titanates are shown in Fig. 14.

The titanates of $La_2Ti_2O_7$ to $Pr_2Ti_2O_7$ are monoclinic built from four modified perovskite subunits, while the titanates $Y_2Ti_2O_7$ and $Nd_2Ti_2O_7$ are representative of the cubic pyrochlore structure. The calculated lattice constants (Table 6) are in agreement with the literature [125,126]. The determined average crystallite sizes are given in Table 6, too. The values are ranging between 91(24) nm for $Nd_2Ti_2O_7$ and 199(49) nm for $Pr_2Ti_2O_7$.

The X-ray diffraction patterns of the prepared rare earth zirconates are depicted in Fig. 15.

The zirconates of $La_2Zr_2O_7$ to $Sm_2Zr_2O_7$ belong to the cubic pyrochlore structure, and $Y_2Zr_2O_7$ is a representative of a random defect fluorite structure. The calculated lattice constants (Table 6) correspond to literature values [122,127]. The crystallite sizes (Table 6) show only small variations and are typically 25 nm. This is in agreement with literature values for via the urea combustion process prepared zirconates, which are in the range of 6.3 nm for $Nd_2Zr_2O_7$ and 50.0 nm for $Y_2Zr_2O_7$ [127].

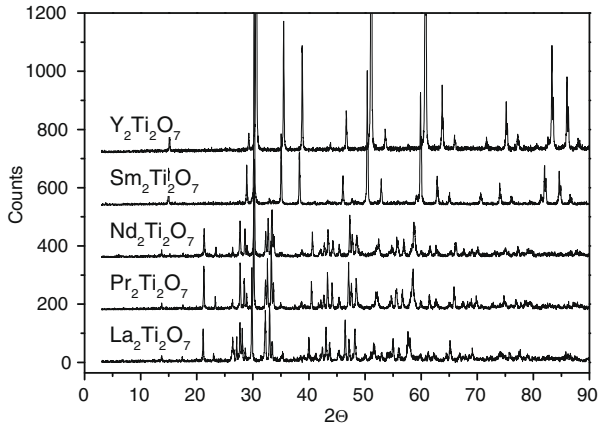

Fig. 14. X-ray powder diffraction patterns of different rare earth titanates.

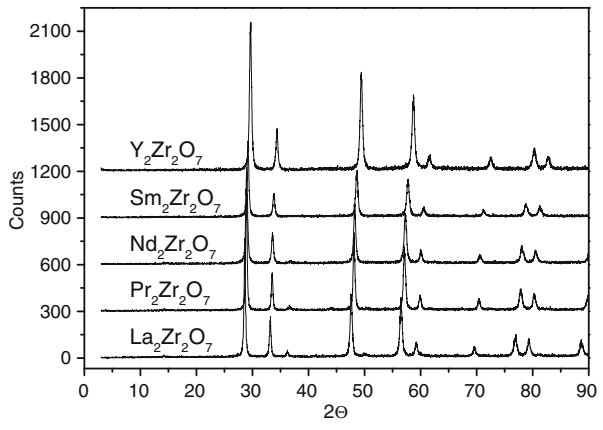

Fig. 15. X-ray powder diffraction patterns of different rare earth zirconates.

The results demonstrate that a great number of potential biodiesel catalysts is accessible via flash combustion synthesis. The combination of different basic rare earth oxides with different weak basic or amphoteric oxides allows a fine tuning of the catalyst properties.

The 15 described catalysts were used for the transesterification of refined palm oil under standard conditions of 50% methanol and 200 °C. Due to the very different crystallite sizes and surface areas, the results cannot be directly compared. For better comparability, the results were related to the specific surface transesterification activity, which is calculated according Eqs. (10)–(12). In case of the aluminates $LaAlO_3$ to $SmAlO_3$, the literature data of the X-ray density [124] was used, all other data is based on our own XRD measurements.

A comparison of the specific surface activities is shown in Fig. 16.

The results are compared by the RE^{3+} ion radius, which allows a better classification of the yttrium compounds. The activity values are based on the initial transesterification rate. Related to this, the aluminates of $LaAlO_3$ to $SmAlO_3$ are of comparatively low activity of typically 0.082 mmol m^{-2} h^{-1}. The structure change of the $Y_3Al_5O_{12}$ garnet results in virtually no activity. The titanates show a continuously increasing activity of 0.101 mmol m^{-2} h^{-1} for $La_2Ti_2O_7$, which culminates at 1.035 mmol m^{-2} h^{-1} for $Y_2Ti_2O_7$. Finally, the zirconates reveal a maximum at an intermediate ion radius with an activity of 0.371 mmol m^{-2} h^{-1} for $Sm_2Zr_2O_7$.

In comparison with the pure rare earth oxides, the mixed oxide catalysts possess much less activity. Reasons are the high crystallinity and low surface area. The best result was obtained with $Sm_2Zr_2O_7$, which gave 58.4% FAME and 43.6% glycerol yield. This catalyst has the best combination of specific activity and surface area. A lot of further optimization potential can be expected.

The value of these investigations is justified by the explanation of the activity tendencies of supported rare earth oxide catalysts, because surface mixed oxides are formed on any oxidic support. In addition, for basic mixed oxides such as the described aluminates, titanates, and zirconates, a much better resistance against soap formation caused by FFA traces in the vegetable oil feed is expected.

However, the results offer valuable information about the most favorable combinations between different oxidic catalyst supports and rare earth oxides. Based on this, extruded catalysts of the most favorable combinations La_2O_3/Al_2O_3, Y_2O_3/TiO_2, and Sm_2O_3/ZrO_2 were prepared. Extrudates of La_2O_3 on activated carbon were made, too. At present, experiments in the continuous trickle-bed

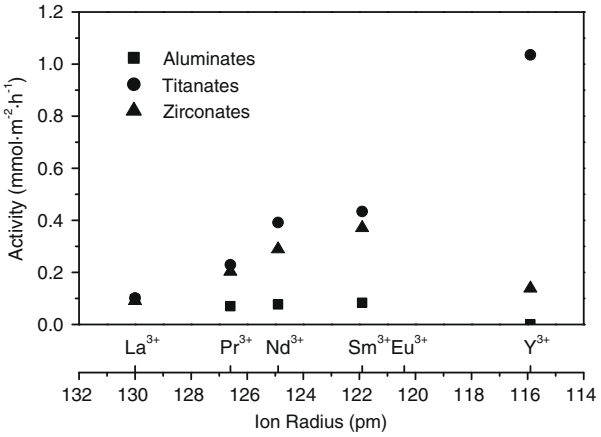

Fig. 16. Specific transesterification activity of different rare earth mixed oxides using refined palm oil and 50% methanol as feed at 200 °C.

mode with these catalysts are underway. Of special interest are the long-term catalyst performance and the influence of catalyst poisons of different plant oils like traces of Na, K, Mg, and Ca as soaps [37] and P bound in phospholipides. Those results will be published soon in an additional paper.

3.8. Activity of La_2O_3 on activated carbon

Activated carbon made from wood (Fluka, analytical grade) was found to be the single catalyst carrier, which stabilizes the La_2O_3 phase. Three different catalysts of 10%, 20%, and 50% La_2O_3 content were prepared by slow precipitation of $LaOH(CO_3)$ on activated carbon, followed by calcination at 900 °C under high vacuum. As far as we know, such kind of catalyst preparation was not reported yet. The X-ray powder diffraction patterns are shown in Fig. 17.

For comparison, the amorphous carbon support and the previously discussed La_2O_3 are shown, too. No substantial impurities like oxycarbonates of the type $La_2O_2(CO_3)$ can be observed. Due to the high XRD detection limits, some minor impurities might be present. The peak widths indicate that an increasing La_2O_3 content is accompanied by an increasing crystallite size. More quantitative, according to Eq. (1), a crystallite size of 29(5) nm for 10%, 41(5) nm for 20%, and 49(7) nm for 50% La_2O_3 content is calculated. The neat La_2O_3 is highly crystalline and exhibits 225(34) nm particle size. Hence, the loading of La_2O_3 on activated carbon leads to a significant improvement of the La_2O_3 dispersion.

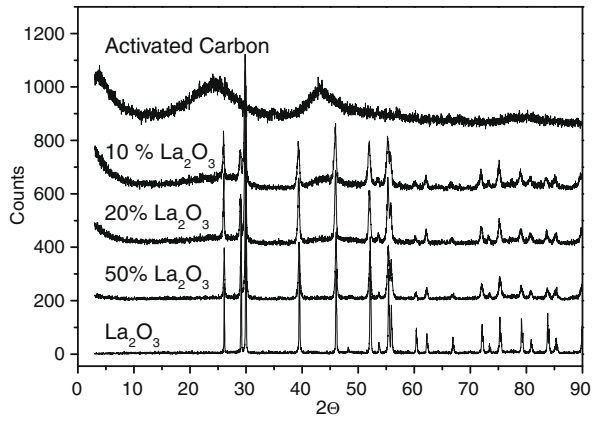

Fig. 17. Effect of the La_2O_3 loading on activated carbon on the X-ray powder diffraction patterns.

The surface properties were further investigated via the nitrogen adsorption isotherms, shown in Fig. 18.

The results show that the loading of La_2O_3 has no effect on the surface area and the pore structure of the activated carbon investigated. In case of 50% La_2O_3 on activated carbon, the BET surface area, micropore area, and BJH mesopore area is cut in half with respect to the carrier. This matches our expectations, because the amount of carrier in the sample is cut in half, too. The mesopore volume decreases from 0.606 $cm^3\,g^{-1}$ for the carrier to 0.322 $cm^3\,g^{-1}$ for 50% La_2O_3, while the average pore diameter remains constant 6.0 nm.

Finally, the dispersal of the La_2O_3 on the activated carbon was investigated by CO_2-TPD measurements, which are shown in Fig. 19.

While the activated carbon is an inert material, successive loading with La_2O_3 leads to an increase in base strength, shifting the CO_2 desorption temperature from 664 °C for 10% La_2O_3 to 688 °C for 20% La_2O_3 and 724 °C for 50% La_2O_3. The desorption peak area increases from 10% to 20% La_2O_3 content, while the specific number of basic centers of 50% La_2O_3 on activated carbon is comparable with 20% La_2O_3 content. Related to the TG measurements shown in Fig. 4, the high desorption temperature can be explained by formation of $La_2O_2(CO_3)$ on the surface and its decomposition at approximately 700 °C. In addition, the smaller desorption signal at typically 450 °C fits well to the transition of $La_2O(CO_3)_2$ to $La_2O_2(CO_3)$.

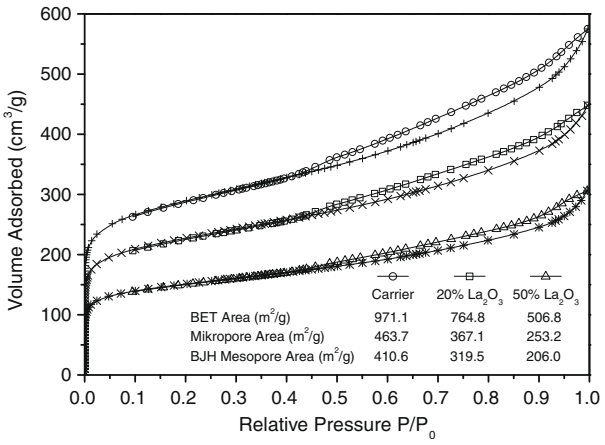

Fig. 18. Effect of the La_2O_3 content supported on activated carbon on the BET surface area, micropore surface area, and BJH mesopore surface area.

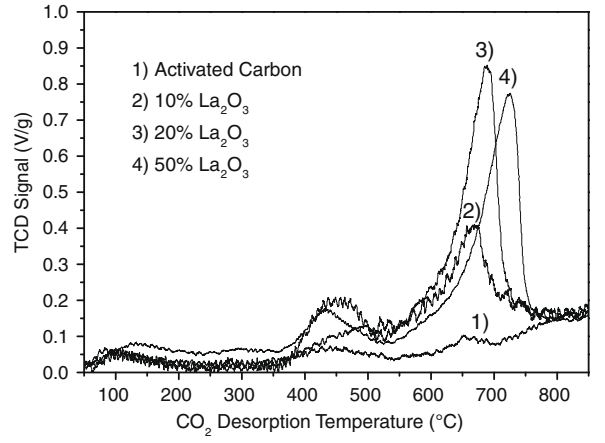

Fig. 19. Effect of the La_2O_3 loading on activated carbon on the temperature-programmed desorption of CO_2.

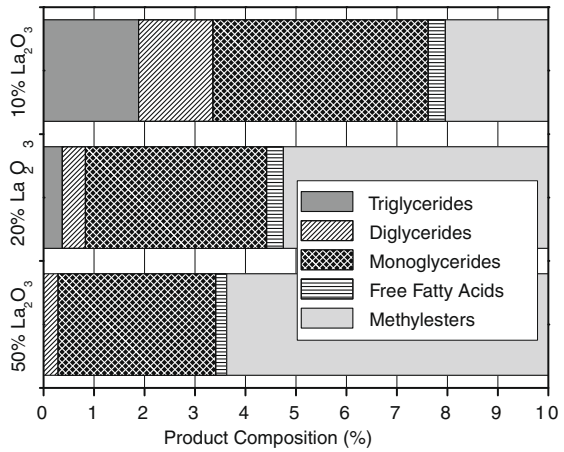

Fig. 20. Residual acylglycerides using refined palm oil and 50% methanol as feed in presence of different La_2O_3 contents loaded on activated carbon at 200 °C. Remaining 90% of palm oil methyl esters are not shown.

The influence of the La_2O_3 loading on the catalytic performance of the transesterification of refined palm oil with 50% methanol at 200 °C is depicted in Fig. 20.

All three investigated catalysts are of excellent activity. In the series 10%, 20%, and 50% La_2O_3 on activated carbon, an increasing palm oil methylester yield is observed, leading to the best result of 96.9% FAME yield at 99.7% selectivity and 92.2% glycerol yield at 94.9% selectivity for the catalyst with 50% La_2O_3. These values are close to the thermodynamic equilibrium under these conditions. The product contains only residual 0.3% diglycerides, 3.1% monoglycerides, 0.2% FFAs, and the bulk is made of 96.4% FAME. With the lower loadings of 20% La_2O_3 95.9% FAME yield and 10% La_2O_3 92.8% FAME yield are obtained. That means even with the lowest La_2O_3 loading of 10% the activity is exceeding the performance of the pure La_2O_3, which is forming 90.6% FAME yield under the same conditions (Fig. 5).

These observations are in good agreement with the XRD measurements. From 10% over 20% and 50% La_2O_3 content, a slight increase in the crystallite size is observed, but the increasing amount of active La_2O_3 by far exceeds this undesirable effect. Furthermore, the CO_2-TPD curves clearly indicate an increasing number of basic sites for the transition of 10% to 20% La_2O_3 loading. However, for 50% La_2O_3, the accessible number of basic sites is comparable, but the base strength increases as indicated by a shift of the CO_2 desorption temperature to higher values.

In conclusion, 50% La_2O_3 supported on activated carbon represents the most active transesterification catalyst of all catalysts investigated in this paper.

4. Conclusions

Nowadays, the rare earth elements are neither rare nor restricted to lab-scale research. In fact, quite the reverse is true. The rare earth elements belong to the longest lasting commodity reserves due to the large known ore deposits in Inner Mongolia, China. Therefore, many applications were opened up and a high future potential is expected.

In this study the rare earth oxides of Y and La to Sm were used for the transesterification of crude and refined palm oil. As expected, the activity is decreasing in the order La to Sm and Y in parallel to the decreasing ion radius and basicity, leading to an excellent activity for La_2O_3. This trend is interrupted by Ce and Pr, which form CeO_2 of almost no activity and Pr_6O_{11} of slightly reduced activity.

In an optimization study of La_2O_3 catalysts in the transesterification of rapeseed oil, the best results of 97.5% FAME and 93.8% glycerol yield were obtained with 50% methanol at 200 °C.

The comparison of crude palm oil with 5.0% FFA and refined, virtually free of FFA palm oil reveals that for crude palm oil always higher oil conversions are obtained. For the blank experiments crude oil yields 9.5% and refined oil only 4.0% FAME. These results can be explained by an auto catalytic acceleration of the reaction rate by the FFA content. However, in case of the most active La_2O_3 catalyst crude oil results in 96.9% but refined oil in only 90.6% FAME yield. These findings indicate an insufficient catalyst stability and a partial homogeneous catalysis by the formation of basic soaps.

In the next step supporting of rare earth oxides on different carriers was investigated in order to improve the catalytic surface and reduce the amount of active compound. Solely activated carbon is an inert carrier, capable to be coated by the rare earth oxides itself. All other investigated oxidic carrier materials are forming surface mixed oxide phases with the rare earth oxides.

Furthermore, a whole series of catalysts made of 10% of each rare earth oxide of La to Yb and Y on γ-Al_2O_3 was prepared and tested with rapeseed oil. The differences are small and the FAME yield is typically in the range 45–70% at 200 °C. In this respect Ce is an exception, which is only partially stabilized as catalytically active $CeAlO_3$ and the remainder consists of inactive CeO_2. In all cases mixed oxides are formed of perovskite structure for La to Gd like $LaAlO_3$ and garnet structure for Y and Dy to Yb. Therefore, the activity is much lower, compared to the pure rare earth oxides. However, a much better resistance towards free fatty acids is expected and at elevated temperature of 250 °C with 10% Pr_2O_3 on γ-Al_2O_3, the top result of 96.8% FAME yield at 99.5% selectivity and 92.6% glycerol yield at 95.2% selectivity is obtained.

For different La_2O_3 on γ-Al_2O_3 coatings an activity maximum at 20% loading is observed, due to the opposite effects of an increasing active compound content but a decreasing BET surface area.

In addition, monoclinic and tetragonal ZrO_2 are more suitable oxidic supports. With refined palm oil and 10% La_2O_3 on monoclinic ZrO_2, 92.5% FAME and 85.2% glycerol yield are formed. In a comparable way for 19% La_2O_3 on tetragonal ZrO_2 92.0% FAME and 85.1% glycerol yield is generated.

The rare earth aluminates $REAlO_3$ for La to Sm and $Y_3Al_5O_{12}$, titanates $RE_2Ti_2O_7$ for La to Sm and Y, and zirconates $RE_2Zr_2O_7$ for La to Sm and Y were successfully prepared by flash combustion synthesis. For most of the compounds unit cell parameters could be determined by powder XRD. For better comparability the activity during the transesterification of refined palm oil was related to the specific catalyst surface area. The following trends of the intrinsic activities can be drawn. For the aluminates $REAlO_3$ for La to Sm a low, but universal activity is found, while $Y_3Al_5O_{12}$ due to the change from the perovskite structure to the garnet structure is inactive. For the titanium compounds $RE_2Ti_2O_7$ the decreasing ion radius in the order La to Sm and Y surprisingly leads to a continuously increasing activity, culminating at $Y_2Ti_2O_7$, which is the most active compound of all investigated stoichiometric mixed oxides. Finally, for the zirconia pyrochlores $RE_2Zr_2O_7$ an intermediate activity and a broad maximum for Pr and Nd is found.

Since the loading of rare earth oxides on any oxidic catalyst carrier always leads to the formation of surface mixed oxide phases, these results allow to predict the best rare earth oxide and oxidic support combinations.

Finally, in case of activated carbon an increasing La_2O_3 loading in the range 10–50 wt.% enhances the catalyst activity. This leads to the top result of 96.9% FAME yield at 99.7% selectivity and 92.2% glycerol yield at 94.9% selectivity with 50% La_2O_3 and refined palm oil.

Currently, continuous experiments with different supported rare earth oxide catalysts are ongoing and the results will be published soon.

Acknowledgments

The support with rapeseed oil by Biowerk Sohland GmbH, Germany and both crude and refined palm oil from ADM Company, Germany is gratefully acknowledged. The authors are especially grateful for the supply of different zirconia precursors by Dr. J. Tunstall, Mel Chemicals, England.

References

[1] L. Plass, S. Reimelt, Chem. Ing. Tech. 79 (2007) 561–568.
[2] R. Luque, L. Herrero-Davila, J.M. Campelo, J.H. Clark, J.M. Hidalgo, D. Luna, J.M. Marinas, A.A. Romero, Energy Environ. Sci. 1 (2008) 542–564.
[3] A. Tilche, M. Galatola, Water Sci. Technol. 57 (2008) 1683–1692.
[4] J. Goldemberg, Science 315 (2007) 808–810.
[5] A. Demirbas, Energy Convers. Manage. 50 (2009) 14–34.
[6] M. Balat, H. Balat, Energy Convers. Manage. 49 (2008) 2727–2741.
[7] B. Smith, H.C. Greenwell, A. Whiting, Energy Environ. Sci. 2 (2009) 262–271.
[8] F. Ma, M.A. Hanna, Bioresour. Technol. 70 (1999) 1–15.
[9] A. Vogel, F. Mueller-Langer, M. Kaltschmitt, Chem. Eng. Technol. 31 (2008) 755–764.
[10] W.N. Rowlands, A. Masters, T. Maschmeyer, Bull. Sci. Technol. Soc. 28 (2008) 149–158.
[11] B. Kamm, M. Kamm, Chem. Ing. Tech. 79 (2007) 592–603.
[12] H. Lyko, G. Deerberg, E. Weidner, J. Biotechnol. 142 (2009) 78–86.
[13] G. Vicente, M. Martínez, J. Aracil, Bioresour. Technol. 92 (2004) 297–305.
[14] U. Rashid, F. Anwar, Fuel 87 (2008) 265–273.
[15] Y.C. Sharma, B. Singh, S.N. Upadhyay, Fuel 87 (2008) 2355–2373.
[16] L.C. Meher, D.V. Sagar, S.N. Naik, Renew. Sustain. Energy Rev. 10 (2006) 248–268.
[17] J.M. Encinar, J.F. González, A. Rodríguez-Reinares, Ind. Eng. Chem. Res. 44 (2005) 5491–5499.
[18] A. Sivasamy, K.Y. Cheah, P. Fornasiero, F. Kemausuor, S. Zinoviev, S. Miertus, Chem. Sus. Chem. 2 (2009) 278–300.
[19] A.P. Vyas, J.L. Verma, N. Subrahmanyam, Fuel 89 (2010) 1–9.
[20] K.G. Cassman, A.J. Liska, Bioprod. Bioref. 1 (2007) 18–23.
[21] J. Kwiecien, M. Hájek, F. Skopal, Bioresour. Technol. 23 (2009) 5555–5559.
[22] A. Behr, J. Eilting, K. Irawadi, J. Leschinski, F. Lindner, Green Chem. 20 (2008) 13–30.
[23] C.-H. Zhou, J.N. Beltramini, Y.-X. Fan, G.Q. Lu, Chem. Soc. Rev. 37 (2008) 527–549.
[24] J.L. Dubois, C. Duquenne, W.F. Hoelderich, FR Patent 2884818 A1, 2005; EP Patent 1874720 A1, 2006; US Patent 2008 183013 A1, 2008; WO Patent 2006 114506 A1, 2006, to Arkema.
[25] W.F. Hölderich, A. Ülgen, DE Patent 10 2008 027 350.3, 2008.
[26] A. Uelgen, W.F. Hoelderich, Catal. Lett. 131 (2009) 122–128.
[27] W.F. Hölderich, M. Schwarzmann, W.D. Mross, Erzmetall 39 (1986) 292–298.
[28] A. Chauvel, B. Delmon, W.F. Hölderich, Appl. Catal. A: Gen. 115 (1994) 173–217.
[29] K. Tanabe, W.F. Hoelderich, Appl. Catal. A: Gen. 181 (1999) 399–434.
[30] W.F. Hölderich, H. van Bekkum, Stud. Surf. Sci. Catal. 137 (2001) 821–910.
[31] W.F. Hölderich, D. Heinz, Catalysis 14 (1999) 149–161.
[32] W.F. Hölderich, Catal. Today 62 (2000) 115–130.
[33] W.F. Hölderich, in: J.M. Lehn et al. (Eds.), Comprehensive Supramolecular Chemistry, Elsevier, England, 1996, pp. 671–692.
[34] T. Dittmar, T. Dimming, B. Ondruschka, B. Heyn, J. Haupt, M. Lauterbach, Chem. Ing. Tech. 75 (2003) 595–601.
[35] T. Dittmar, T. Dimming, B. Ondruschka, B. Heyn, J. Haupt, M. Lauterbach, Chem. Ing. Tech. 75 (2003) 601–608.
[36] M. Canakci, J. Van Gerpen, Trans. ASAE 44 (2001) 1429–1436.
[37] B.M.E. Russbueldt, W.F. Hoelderich, Appl. Catal. A: Gen. 362 (2009) 47–57.
[38] Y. Feng, B. He, Y. Cao, J. Li, M. Liu, F. Yan, X. Liang, Bioresour. Technol. 101 (2010) 1518–1521.
[39] J.-Y. Park, D.-K. Kim, J.-S. Lee, Bioresour. Technol. 101 (2010) S62–S65.
[40] Y. Liu, L. Wang, Y. Yan, Fuel Process. Technol. 90 (2009) 857–862.
[41] R. Stern, G. Hillion, J.-J. Rouxel, S. Leporq, US Patent 5908946, 1999, to Institut Francais du Petrole.
[42] L. Bournay, G. Hillion, P. Boucot, J.-A. Chodorge, C. Bronner, A. Forestiere, US Patent 6878837, 2005, to Institut Francais du Petrole.
[43] M. Bloch, L. Bournay, D. Casanave, J.A. Chodorge, V. Coupard, G. Hillion, D. Lorne, Oil Gas Sci. Technol. 63 (2008) 405–417.
[44] R. Rinaldi, F. Schüth, Energy Environ. Sci. 2 (2009) 610–626.
[45] Z. Helwani, M.R. Othman, N. Aziz, J. Kim, W.J.N. Fernando, Appl. Catal. A: Gen. 363 (2009) 1–10.
[46] M. Zabeti, W. Mohd, A.W. Daud, M.K. Aroua, Fuel Process. Technol. 90 (2009) 770–777.
[47] X. Liu, X. Piao, Y. Wang, S. Zhu, J. Phys. Chem. A (2009), doi:10.1021/jp9039379.
[48] K. Huang, Q. Xu, S. Zhang, Z. Ren, Y. Yan, Chem. Eng. Technol. 32 (2009) 1–11.
[49] K. Noiroy, P. Intarapong, A. Luengnaruemitchai, J.-I. Samai, Renew. Energy 34 (2009) 1145–1150.
[50] A. D'Cruz, M.G. Kulkarni, L.C. Meher, A.K. Dalai, J. Am. Oil Chem. Soc. 84 (2007) 937–943.
[51] C.S. MacLeod, A.P. Harvey, A.F. Lee, K. Wilson, Chem. Eng. J. 135 (2008) 63–70.
[52] W. Xie, H. Peng, L. Chen, Appl. Catal. A: Gen. 300 (2006) 67–74.
[53] C. Lingfeng, X. Guomin, X. Bo, T. Guangyuan, Energy Fuels 21 (2007) 3740–3743.
[54] W. Xie, H. Li, J. Mol. Catal. A: Chem. 225 (2006) 1–9.
[55] T. Wan, P. Yu, S. Wang, Y. Luo, Energy Fuels 23 (2009) 1089–1092.
[56] S. Banjapornkulaphong, C. Ngancharussrivichai, K. Bunyakiat, Chem. Eng. J. 145 (2009) 468–474.
[57] M. Verziu, M. Florea, S. Simon, V. Simon, P. Filip, V.I. Parvulescu, C. Hardacre, J. Catal. 263 (2009) 56–66.
[58] S. Gryglewicz, Bioresour. Technol. 70 (1999) 249–253.
[59] M. Kouzu, T. Kasuno, M. Tajika, Y. Sugitomo, S. Yamanaka, J. Hidaka, Fuel 87 (2008) 2798–2806.
[60] C.R. Venkat, R. Oshel, J.G. Verkade, Energy Fuels 20 (2006) 1310–1314.
[61] M.L. Granados, M.D.Z. Poves, D.M. Alonso, R. Mariscal, F.C. Galistero, R. Moreno-Tost, J. Santamaría, Appl. Catal. B: Environ. 73 (2007) 317–326.
[62] M.L. Granados, D.M. Alonso, I. Sádaba, R. Mariscal, P. Ocón, Appl. Catal. B: Environ. 89 (2009) 265–272.
[63] M. Kouzu, S. Yamanaka, Y. Hidaka, M. Tsunomori, Appl. Catal. A: Gen. 355 (2009) 94–99.
[64] M. Verziu, B. Cojocaru, J. Hu, R. Richards, C. Ciuculescu, P. Filip, V.I. Parvulescu, Green Chem. 10 (2008) 373–381.
[65] J.M. Montero, P. Gai, K. Wilson, A.F. Lee, Green Chem. 11 (2009) 265–268.
[66] K. Elst, W. Adransens, L. Willems, L. Van Ginneken, WO Patent 2008/012275, 2008, to Vlaamse Instelling Voor Technologisch Onderzoek.
[67] D.G. Cantrell, L.J. Gillie, A.F. Lee, K. Wilson, Appl. Catal. A: Gen. 287 (2005) 183–190.
[68] H.-Y. Zeng, Z. Feng, X. Deng, Y.-Q. Li, Fuel 87 (2008) 3071–3076.
[69] E. Li, Z.P. Xu, V. Rudolph, Appl. Catal. B: Environ. 88 (2009) 42–49.
[70] M. Zabeti, W. Mohd, A.W. Daud, M.K. Arouda, Appl. Catal. A: Gen. 366 (2009) 154–159.
[71] A. Kawashima, K. Matsubara, K. Honda, Bioresour. Technol. 99 (2008) 3439–3443.
[72] D.M. Alonso, R. Mariscal, M.L. Granados, P.M. Maireles-Torres, Catal. Today 143 (2009) 167–171.
[73] X. Liang, S. Gao, J. Yang, M. He, Renew. Energy 34 (2009) 2215–2217.
[74] X. Li, G. Lu, Y. Guo, Y. Guo, Y. Wang, Z. Zhang, X. Liu, Y. Wang, Catal. Commun. 8 (2007) 1969–1972.
[75] H. Sun, K. Hu, H. Lou, X. Zheng, Energy Fuels 22 (2008) 2756–2760.
[76] N.S. Babu, R. Sree, P.S.S. Prasad, N. Lingaiah, Energy Fuels 22 (2008) 1965–1971.
[77] S. Yan, M. Kim, S.O. Salley, K.Y.S. Ng, Appl. Catal. A: Gen. 360 (2009) 163–170.
[78] S. Yan, S.O. Salley, K.Y.S. Ng, Appl. Catal. A: Gen. 353 (2009) 203–212.
[79] J.M. Rubio-Caballero, J. Santamaría-González, J. Mérida-Robles, R. Moreno-Tost, A. Jiménez-López, P. Maireles-Torres, Appl. Catal. B: Environ. 91 (2009) 339–346.
[80] F.R. Abreu, M.B. Alvez, C.C.S. Macêdo, L.F. Zara, P.A.Z. Suarez, J. Mol. Catal. A: Chem. 227 (2005) 263–267.
[81] C.C.S. Macedo, F.R. Abreu, A.P. Tavares, M.B. Alves, L.F. Zara, J.C. Rubim, P.A. Suarez, J. Brazil Chem. Soc. 17 (2006) 1291–1296.
[82] G.J. Suppes, M.A. Dasari, E.J. Doskocil, P.J. Mankindy, M.J. Goff, Appl. Catal. A: Gen. 257 (2004) 213–223.
[83] A.Z.A.N. Razali, K.T. Lee, Fuel Process. Technol. 90 (2009) 958–964.
[84] C.R. Bayense, H. Hinnekens, J. Martens, US Patent 5508457, 1996, to Engelhard De Meern and Fina Research.
[85] U. Schuchardt, R.M. Vargas, G. Gelbard, J. Mol. Catal. A: Chem. 109 (1996) 37–44.
[86] N. Shibasaki-Kitakawa, H. Honda, H. Kuribayashi, T. Toda, T. Fukumura, T. Yonemoto, Bioresour. Technol. 98 (2007) 416–421.
[87] Y. Toshikuni, K. Naowi, T. Takuji, JP Patent 2006-104316, A, 2006.
[88] O. Ilgen, A.N. Akin, N. Boz, Turk. J. Chem. 33 (2009) 289–294.
[89] S.K.F. Peter, R. Ganswindt, H.-P. Neuner, E. Weidner, Eur. J. Lipid Sci. Technol. 104 (2002) 324–330.
[90] S. Peter, E. Weidner, H.-P. Neuner, R. Ganswindt, US Patent 6359157, 2002.
[91] S. Zheng, M. Kates, M.A. Dubé, D.D. McLean, Biomass Bioenergy 30 (2006) 267–272.
[92] S.C.M. dos Reis, E.R. Lachter, R.S.V. Nascimento, J.A. Rodriguez Jr., M.G. Reid, J. Am. Oil. Chem. Soc. 82 (2005) 661–665.
[93] C.M. Garcia, S. Teixeira, L.L. Marciniuk, U. Schuchardt, Bioresour. Technol. 99 (2008) 6608–6613.
[94] K. Suwannakarn, E. Lotero, J.G. Goodwin Jr., J. Catal. 225 (2008) 279–286.
[95] G. Sunita, B.M. Devassy, A. Vinu, D.P. Sawant, V.V. Balasubramanian, S.B. Halligudi, Catal. Commun. 9 (2008) 696–702.
[96] M.G. Kulkarni, R. Gopinath, L.C. Meher, A.K. Dalai, Green Chem. 8 (2006) 1056–1062.
[97] L. Pesaresi, D.R. Brown, A.F. Lee, J.M. Montero, H. Williams, K. Wilson, Appl. Catal. A: Gen. 360 (2009) 50–58.
[98] J. Li, X. Wang, W. Zhu, F. Cao, Chem. Sus. Chem. 2 (2009) 177–183.
[99] V.V. Bokade, G.D. Yadav, Process Saf. Environ. Prot. 85 (2007) 372–377.
[100] J. Kansedo, K.T. Lee, S. Bhatia, Biomass Bioenergy 33 (2009) 271–276.
[101] S. Furuta, H. Matsuhashi, K. Arata, Biomass Bioenergy 30 (2006) 870–873.

[102] H. Fukuda, A. Kondo, H. Noda, J. Biosci. Bioeng. 92 (2001) 405–416.
[103] H. Fukuda, H. Noda, US Patent 6982155, 2006, to Kansei Chemical Engineering.
[104] L. Fjerbaek, K.V. Christensen, B. Norddahl, Biotechnol. Bioeng. 102 (2009) 1298–1315.
[105] M. Kaieda, T. Samukawa, A. Kondo, H. Fukuda, J. Biosci. Bioeng. 91 (2001) 12–15.
[106] Y. Watanabe, Y. Shimada, A. Sugihara, Y. Tominaga, J. Mol. Catal. B: Enzym. 17 (2002) 151–155.
[107] D.G.B. Boocock, US Patent 6642399, 2003.
[108] D.M. Ginosar, R.V. Fox, US Patent 6887283, 2005, to Bechtel BWXT Idaho.
[109] D. Kusdiana, S. Saka, Fuel 80 (2001) 693–698.
[110] T. Sasaki, T. Suzuki, F. Okada, US Patent 6187939, 2001, to Sumitomo Chemical Company.
[111] C. Plank, E. Lorbeer, J. Chromatogr. A 697 (1995) 461–468.
[112] M. Diasakou, A. Louloudi, N. Papayannakos, Fuel 77 (1998) 1297–1302.
[113] E. Minami, S. Saka, Fuel 85 (2006) 2479–2483.
[114] H. Bergmann (Ed.), Gmelin Handbook of Inorganic Chemistry, Sc, Y, La–Lu Rare Earth Elements: Hydrides, Oxides, eighth ed., Springer, Heidelberg, 1974, pp. 205–219 (Syst. Nr. 39 C 1).
[115] T. Moeller, E. Schleitzer-Rust (Eds.), Gmelin Handbook of Inorganic Chemistry, Sc, Y, La-Lu Rare Earth Elements: Complexes and Salts of Carboxylic Acids, Hydrocarboxylic Acids and Esters of Carboxylic Acids, eighth ed., Springer, Heidelberg, 1984, pp. 112–149 (Syst. No. 39 D 5).
[116] H. Bergmann, C. Kloeppel, H. Pscheidl, E. Warkentin (Eds.), Gmelin Handbook of Inorganic and Organometallic Chemistry, Rare Earth Elements: Compounds with Carbon, eighth ed., Springer, Heidelberg, 1994, pp. 152–226 (Syst. No. 39 C 12b).
[117] H. Hattori, Chem. Rev. 95 (1995) 537–558.
[118] Y. Kanke, A. Navrotsky, J. Solid State Chem. 14 (1998) 424–436.
[119] R.C. Garvie, J. Phys. Chem. 82 (1978) 218–224.
[120] B.C. Weber, J. Am. Ceram. Soc. 45 (1962) 614–615.
[121] J.J. Kingsley, K. Suresh, K.C. Patil, J. Solid State Chem. 87 (1990) 435–442.
[122] N.A. Dhas, K.C. Patil, J. Mater. Chem. 3 (1993) 1289–1294.
[123] S. Geller, V.B. Bala, Acta Crystallogr. 9 (1956) 1010–1025.
[124] T. Shishido, S. Nojima, M. Tanaka, H. Horiuchi, T. Fukuda, J. Alloys Compd. 227 (1995) 175–179.
[125] L.H. Brixner, Inorg. Chem. 3 (1964) 1065–1067.
[126] D.W. Hwang, J.S. Lee, W. Li, S.H. Oh, J. Phys. Chem. B 107 (2003) 4963–4970.
[127] A. Zhang, M. Lü, Z. Yang, G. Zhou, Y. Zhou, Solid State Sci. 10 (2008) 74–81.